Geochemistry, Geophysics, Geosystems

RESEARCH ARTICLE
10.1029/2018GC007593

Elemental Systematics in MORB Glasses From the Mid-Atlantic Ridge

Shuying Yang[1], **Munir Humayun**[1], **and Vincent J. M. Salters**[1]

[1]National High Magnetic Field Laboratory and Department of Earth, Ocean and Atmospheric Science, Florida State University, Tallahassee, FL, USA

Key Points:
- We present a new set of elemental analysis of 60 elements in 319 MORB glasses by LA-ICP-MS
- A recycled crustal origin for the enrichment of MORBs is not supported by elemental ratios sensitive to processing in the subduction factory
- All MORB glasses have identical depletions of As, Tl, Pb, and Bi, complementary to the continental crust acquired early in Earth history

Supporting Information:
- Supporting Information S1
- Table S1

Correspondence to:
M. Humayun,
humayun@magnet.fsu.edu

Citation:
Yang, S., Humayun, M., & Salters, V. J. M. (2018). Elemental systematics in MORB glasses from the Mid-Atlantic Ridge. *Geochemistry, Geophysics, Geosystems*, *19*. https://doi.org/10.1029/2018GC007593

Received 3 APR 2018
Accepted 8 OCT 2018
Accepted article online 13 OCT 2018

Abstract In this study, a data set of 60 elements in 319 mid-oceanic ridge basalt (MORB) glasses representing 144 chemically distinct lava flows from the Mid-Atlantic Ridge was acquired by laser ablation inductively coupled plasma mass spectrometry. Our new data are comparable in terms of the number of elements analyzed to several recent MORB data sets, albeit limited in geographic coverage to the North Mid-Atlantic Ridge. This extensive data set was used to examine the elemental systematics of depleted (D)-, normal (N)-, and enriched (E)-MORBs. We show that elemental ratios sensitive to fluid transport in subduction zones (e.g., Th/U, Nb/U, Ba/Th, and Ba/La) are constant and similar to their primitive mantle values in N- and E-MORBs, but depleted in accordance with their compatibility in D-MORBs. The absence of evidence for subduction zone processing indicates the need to reassess the relation between MORB enrichment and recycled materials. Additionally, we reexamined the ratios of chalcophile and siderophile elements to lithophile elements of comparable compatibility, which are important in assessing planetary accretion, core formation, crust-mantle differentiation, and hydrothermal ore formation processes. MORBs show significant negative anomalies of As, Tl, Pb, and Bi, but not of Sb, relative to lithophile elements of similar compatibility, which cannot be accounted for by melt depletion alone. The depletions of As, Tl, Pb, and Bi in MORB are complementary to significant enrichments observed in the continental crust, indicating that they have been transferred to the continental crust via fluid mobility in arcs or obduction of seafloor hydrothermal ores.

1. Introduction

The composition of mid-oceanic ridge basalts (MORBs) is an important parameter in understanding the Earth's bulk composition, evaluating the evolution and differentiation of the geochemical reservoirs on Earth, and documenting the role of recycled material in the mantle (e.g., Hirschmann & Stolper, 1996; Hofmann, 1988; Langmuir et al., 1993; Niu & O'Hara, 2009; Stracke, 2012; Sun & McDonough, 1989). The abundances of chalcophile and siderophile elements in the Earth's mantle additionally reflect processes of accretion, volatile element depletion, core formation, and late accretion (e.g., Ballhaus et al., 2013; Mann et al., 2009; Righter et al., 2010, 2015; Wade et al., 2012; Wood et al., 2014; Yang et al., 2015). MORBs sample ambient upper mantle, chemically complementary to the incompatible element-enriched continental crust, as partial melts subsequently modified by magma chamber processes (e.g., Coogan & O'Hara, 2015; Shorttle et al., 2016). Based on the abundances of incompatible elements MORBs can be categorized into enriched- (E-), normal- (N-), and depleted- (D-) MORBs (Gale et al., 2013; Perfit, 2001; Schilling, 1973). In a pioneering study, Schilling (1973) found MORBs erupted along the Reykjanes ridge (North Mid-Atlantic Ridge) to be enriched in incompatible elements by the adjacent Iceland plume. E-MORBs were thus used to discriminate plume-related MORBs from common N-MORBs that are incompatible element depleted. Based on a detailed compilation of global MORB data, Gale et al. (2013) showed that E-MORBs $>$ 500 km from plumes are far more common along the mid-oceanic ridge system than previously thought. Models for the formation of E-MORBs far from plumes include the incorporation of recycled oceanic crust (e.g., Hirschmann & Stolper, 1996), plume heads (e.g., Hémond et al., 2006), deep portion of oceanic lithosphere (e.g., Niu et al., 2002), or delaminated subcontinental lithosphere (e.g., Galer & O'Nions, 1986) in depleted MORB mantle (DMM), or the enrichment of DMM by low-degree melts from subducted oceanic crust (e.g., Donnelly et al., 2004).

While the compositions of major elements and lithophile trace elements in the MORBs were extensively studied in prior work (e.g., Gale et al., 2013, 2014; Langmuir et al., 1993; Niu & O'Hara, 2008; Sun & McDonough, 1989), the concentrations of chalcophile (with the exception of Pb) and siderophile elements

in the MORBs were not adequately discussed due to a dearth of relevant information. For example, most chalcophile and siderophile elements (e.g., As, Ge, In, Sb, Cd, Re, and Bi) were not included in the global MORB compilation of Gale et al. (2013), since these elements were not frequently analyzed in geochemical studies. Two recent studies provided a broad suite of elemental abundances in MORBs: Jenner and O'Neill (2012) reported about 60 elements in ~600 ocean floor basalts, including ~500 MORB glasses from the Smithsonian volcanic glass collection, and Kelley et al. (2013) reported 40 trace elements in ~600 MORBs from plume-influenced ridge segments. However, many ratios (e.g., Cd/Dy, Sb/Ce, and Rb/Tl, W/U) constrained using the MORB data from these two studies are mutually inconsistent (Kelley et al., 2013).

To address deficiencies in our knowledge of chalcophile and siderophile element abundances of MORBs, we have precisely analyzed about 60 elements, including major elements, lithophile elements including rare earth elements (REEs), first row transition elements (FRTEs), chalcophile and siderophile elements in 319 MORB glasses representing 144 distinct lava flows from the Mid-Atlantic Ridge (MAR) and Mid-Cayman Rise (MCR). We show that the compositional diversity of our geographically limited MORB samples is representative of the global compositional spectrum of MORB recognized by Gale et al. (2013), covering the depleted (D)-, normal (N)-, and enriched (E)-MORBs. In this paper, we examine the systematics of D-, N-, and E-MORBs using the lithophile trace element ratios (e.g., Th/U, Nb/U, Ba/Th, and Ba/La) that are sensitive to modification by fluids in subduction zone processes. Using this data set, we tested the hypotheses for the genesis of enrichment in MORBs. We used this large data set to better constrain the ratios of chalcophile and siderophile elements to the lithophile elements with similar compatibilities. The complementary compositional relationship of chalcophile and siderophile element abundances between the MORBs and the continental crust are discussed.

2. Materials and Methods

In this study, 319 MORB glasses from the MAR 10°–40°N and MCR 80°W (Figure 1) were analyzed using laser ablation inductively coupled plasma mass spectrometry (LA-ICP-MS). All samples analyzed are MORB glasses obtained from the Smithsonian Seafloor Rock Collection, which were received as polished epoxy discs containing MORB glass chips with the Smithsonian VG 2 glass standard in each mount. It is important to note that, since multiple samples were usually collected from a single dredge, some MORB analyses of this study may be replicate analyses of the same lava flow, a fact that was distinguished by dividing the chips into *chemical groups* based on homogeneity of major element analyses (Melson et al., 1976, 2002). Using the assignments of glass chips to the chemical group numbers in the Smithsonian Abyssal Volcanic Glass Data File (AVGDF; Melson et al., 2002), the 319 MORB glass chips analyzed in this study belong to 144 distinct chemical groups, interpretable as representing 144 distinct MORB lava flows. Using fracture zones (FZ) as offsets, we further divided the MORB lava flows into 11 groups based on their localities (Figure 1), including Valley and the French-American Mid-Ocean Undersea Study (AMAR-FAMOUS, $n = 36$), north ($n = 1$) and south ($n = 1$) of Hayes FZ, south of Kane FZ ($n = 25$), 16.8°N MAR ($n = 1$), north ($n = 35$) and south ($n = 20$ of 15°20 FZ, north ($n = 4$) and south ($n = 1$) of Vema FZ, and Mid-Cayman Rise (MCR, $n = 16$). A few samples ($n = 4$) measured in this study are from South MAR, including AMAR 8.7°S ($n = 1$) and 16°–22°S MAR ($n = 3$). A comprehensive dataset of 60 elements in ~500 MORB oceanic basaltic glasses from the Seafloor Rock Collection was produced by Jenner and O'Neill (2012), however there is no overlap between samples analyzed in this study and those reported in Jenner and O'Neill (2012; Figure 1), except that we have both analyzed VG 2, a glass used as the calibration material of the AVGDF (Melson et al., 2002). The ~600 MORBs analyzed represent an unknown number of flows since Jenner and O'Neill (2012) did not group their glasses into *chemical groups* according to the criteria of Melson et al. (2002).

In this study, all samples were measured using the high-resolution Thermo Finnigan Element XR™ ICP-MS equipped with an Electro Scientific Industries New Wave™ UP-193FX ArF (193 nm) excimer laser ablation system at the Plasma Analytical Facility of the National High Magnetic Field Laboratory, Florida State University (Humayun, 2012; Humayun et al., 2010; Yang et al., 2015). Sample aerosol produced by laser ablation is swept into the mass spectrometer using a stream of ultrahigh purity He gas (800 ml/min). A stream of Ar gas is added downstream, and the flow rate of this gas is tuned for signal optimization on the ICP-MS. In this study, MORB glasses were ablated using 150 μm spot sizes at 50 Hz repetition rate for 20 s per spot. Each sample or standard was ablated at five different spots and the results averaged.

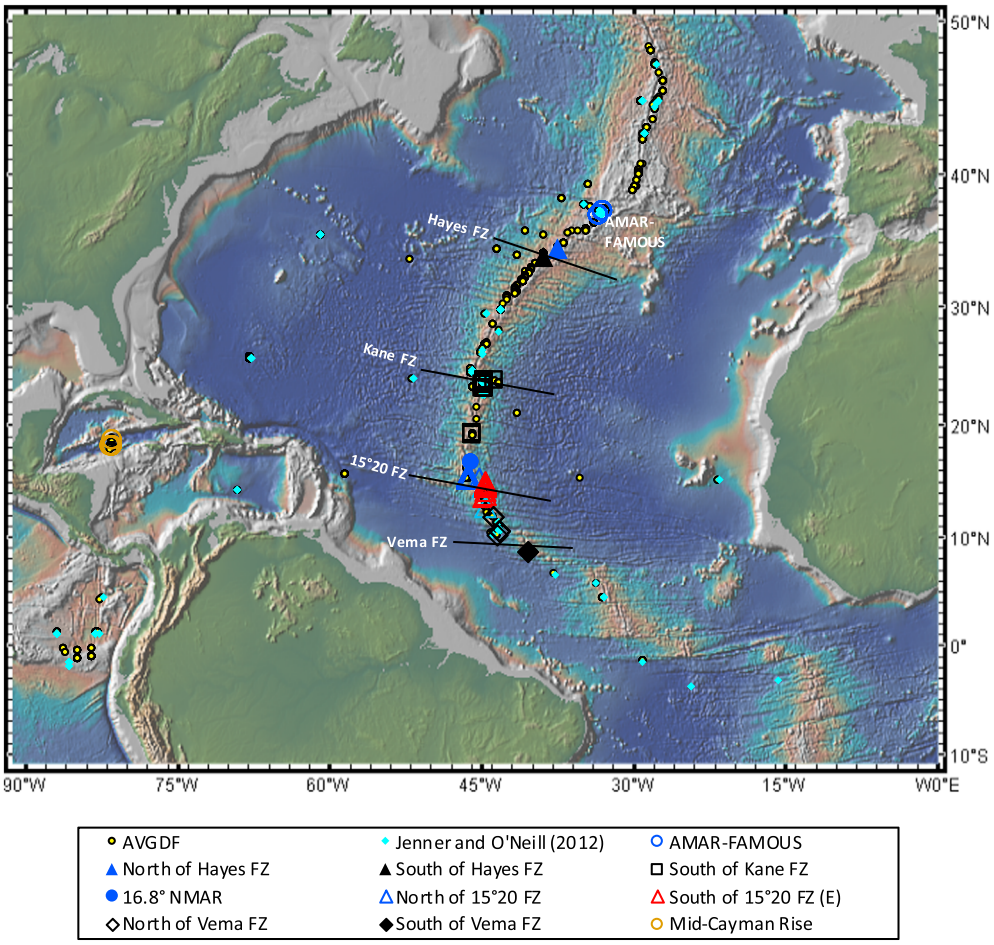

Figure 1. Locations of samples analyzed in this study together with samples analyzed in Jenner and O'Neill (2012) and samples compiled in AVGDF from the same area. Samples from this study are color coded as black: D-MORB; blue: N-MORB, and red: E-MORB. Classifications of MORBs are shown in Figure 2. Based map was custom generated by GeoMapApp (http://www.geomapapp.org). D = depleted; N = normal; E = enriched; MORB = mid-oceanic ridge basalt; AVGDF = Abyssal Volcanic Glass Data File; NMAR = North Mid-Atlantic Ridge; FZ = fracture zones; AMAR-FAMOUS = Valley and the French-American Mid-Ocean Undersea Study.

Mass peaks acquired are listed in Table S1 in the supporting information. Each peak was monitored by electrically scanning the acceleration voltage (EScan mode) over a 15% mass range followed by magnet jumps to cover the mass spectrum from 6 to 238. All peaks were acquired by peak jumping between peak tops with 10% mass window and 50 ms of acquisition time on the peak top for 20 s for each spot. The Element XR™ is equipped with two detectors, a Faraday Cup and a Dual Mode (analog and ion counting) Secondary Electron Multiplier (SEM), of which only the SEM in analog ($>10^6$ cps) or ion counting mode ($<10^6$ cps) was employed. Isotope peaks were collected in low resolution (M/ΔM = 300) with Analog mode detection for major elements and Triple mode detection (effectively ion counting or analog) for other measured elements. Analyses were only undertaken >30 min after each sample disc exchange to ensure background counts, and oxide production rates were minimal during data collection.

To apply corrections for double charged ion interferences affecting the mass region of Zn-Se (Table S1), the doubly charged odd isotopes $^{137}Ba^{++}$, $^{145}Nd^{++}$, and $^{149}Sm^{++}$ were monitored at m/e = 68.5, 72.5, and 74.5 in each spectrum collected (Yang et al., 2015). Measured ^{120}Sn intensity was used to correct the interference of ^{115}Sn on ^{115}In. The interference of $^{91}Zr^{16}O$ on ^{107}Ag was corrected by estimating the $^{90}Zr^{16}O$ from the difference between ^{105}Pd and ^{106}Pd (neglecting CuAr interferences on ^{105}Pd), and then calculating $^{91}Zr^{16}O$ by multiplying by the isotopic ratio of $^{91}Zr/^{90}Zr$. Isotopic abundances were taken from De Bievre and Taylor (1993).

Background intensities measured with the laser off were subtracted from elemental peak intensities and then converted to elemental ratios with respect to SiO_2 by multiplying by the relative sensitivity factors (RSF) obtained from analysis of standards (Humayun et al., 2007):

$$\mathrm{RSF} = \frac{C_i/C_{\mathrm{SiO_2}}}{I_i/I_{29_{\mathrm{Si}}}}$$

where C_i is the preferred value of element or oxide i in the external standard, and I_i is the intensity of the isotope peak of that element. The choices of the external standards for each element are described below, and the standards used for each element are given in Table S1, along with the reference values used for these calibration materials.

The elemental concentrations were calculated by multiplying the elemental ratios with SiO_2 contents obtained from the major element procedure (Humayun et al., 2010):

$$\mathrm{SiO_2} = \frac{100}{\sum \frac{x_i}{\mathrm{SiO_2}}}$$

where x_i are all major oxides, including SiO_2. Accordingly, the major oxides of Na, Mg, Al, Si, P, K, Ca, Ti, Mn, and Fe are normalized to 100 wt. %. Some minor elements, including S, Cr, and Ni, and volatiles not determined in this study (e.g., H_2O), are not included in the summation.

In this study, major elements (excluding FeO_T and MnO) were calibrated against VG 2 a MORB glass dredged from the median valley of the Juan de Fuca Ridge, for internal consistency with major MORB databases, such as the Smithsonian AVGDF (Melson et al., 2002). A piece of VG 2 is mounted with each of the MORB glass sample suites. Thus, VG 2 was analyzed 23 times during the course of analyses of the MORB glasses. Wet chemical abundances for the major elements from Jarosewich (1975) were used for calibration, except for MgO. The MgO content of the wet chemical analysis of VG 2 used to calibrate the abundances was revised from 6.71 wt.% (Jarosewich, 1975) to 6.95 wt. % (Helz et al., 2014) for consistency with other recent glass analyses (Clague et al., 1990; Dixon et al., 1991; Stolper et al., 2004). FeO_T and MnO were calibrated against United States Geological Survey (USGS) standards (BHVO-2g, BCR-2g, and BIR-1g) to obtain Fe/Mn ratios that are traceable to high-precision ICP-MS data (Qin & Humayun, 2008).

In this study, the USGS glasses (BHVO-2g, BCR-2g, and BIR-1g) were used as external standards for elements that have been precisely determined in these glasses, for example, FRTEs, Rb, Sr, Nb, Zr, Ba, REEs, Th, and U. For elements that are either poorly known or low in abundance in USGS glasses, such as Li, Be, B, As, Ga, Ge, Ag, Mo, In, Sn, W, and Tl, NIST SRM 610 (Jochum et al., 2011) was used as the sole standard since matrix-dependent elemental fractionation is less intense in SRM 610 than in SRM 612 (Gaboardi & Humayun, 2009). The MPI-DING glasses (Jochum et al., 2006) were analyzed once to validate the methods. The correlations of Cd to Dy (Yi et al., 2000) and of Sb to Pr (Jochum & Hofmann, 1997) were not observed when using NIST SRM 610 as the external standard to calibrate Cd and Sb. Since both Cd and Sb have FIP $>$ 8 eV, matrix effects between SRM 610 and basaltic glasses are implicated (Gaboardi & Humayun, 2009). Retroactively, Cd and Sb had to be calibrated against USGS glass standards. In GeoReM, the Sb content is given as information values for all three USGS glasses and all MPI-DING glasses, except for KL-2g that has a certified value. A bootstrap method was then applied where USGS glasses were treated as unknowns in the analytical session where KL-2g had been analyzed. The resulting provisional Sb determined for BCR-2g (0.31 ppm) and BIR-1g (0.53 ppm) are within the uncertainty of their GeoReM values (BCR-2g: 0.35 ± 0.08 ppm; BIR-1g: 0.56 ± 0.08 ppm), while Sb determined for BHVO-2g (0.11 ppm) is 3 times lower than its GeoReM value (0.3 ppm). Among eight analyses of Sb in BHVO-2g compiled in GeoReM, only one from Jochum et al. (2005) is higher than 0.3 ppm while others vary from 0.12 to 0.21. The revised Sb abundances of BCR-2g and BIR-1g were then applied to calibrate Sb in all of the MORB samples analyzed in this study. Since a certified value of Cd is not available for any of the USGS or MPI-DING glasses, the information values were used to obtain RSFs for Cd (Table S1). A future improvement in accuracy is possible with the development of new Cd abundance standards since our data are linearly dependent on the abundance in the standard.

3. Results

Concentrations of 60 elements in 319 MORB glasses, and the individual replicate analyses of VG 2, USGS glass standards, and MPI-DING glass standards analyzed in this study are given in Table S1, together with the isotope used, the detection limits, the interferences corrected, the standards used to calibrate the concentrations, and the concentration data for the standards. At the high beam intensity (150 μm, 50 Hz) used in this study, the variability of the blanks contributed negligibly to the precision of the measurements of most elements included in our analytical routine, except Se, Ru, Rh, Te, Os, Ir, Pt, and Au that had concentrations below their detection limits in MORB glasses. Alkalis, particularly Li and Cs, showed a strong *memory effect* (residual signal carryover from sample to sample), which consequently contributed to high and variable backgrounds, resulting in analyses that are below detection limit for some samples (Table S1). The average compositions of the chemical groups representing distinct MORB lava flows are given in Table S2 and are plotted in the figures of this manuscript. In this section, we will first assess the precision and accuracy of MORB data obtained in this study.

3.1. Evaluating Data Precision and Accuracy

For those major and trace elements that were not standardized to USGS glasses, their abundances in the three USGS glasses (BHVO-2g, BCR-2g, and BIR-1g) measured repeatedly (n = 14) in this study are given in Table S1. The analytical precision is better than 4% (1σ) for major elements, except for K_2O in BIR-1g. Major element compositions of USGS glasses determined in this study are in good agreement with GeoReM-preferred values (Jochum & Nohl, 2008) within uncertainties, except for minor elements Na_2O, P_2O_5, K_2O, and TiO_2. The Na_2O contents determined in this study are 6% lower for BCR-2g and BIR-1g and 12% lower for BHVO-2g than the GeoReM-preferred values. The P_2O_5 contents determined in this study are ~10% lower for both BHVO-2g and BCR-2g and 31% lower for BIR-1g than the GeoReM-preferred values. The K_2O contents determined in this study are ~20% higher for BHVO-2g, similar for BCR-2g and 18% lower for BIR-1g than the GeoReM-preferred values. The TiO_2 contents determined in this study are similar to GeoREM values for both BHVO-2g and BCR-2g but 9% lower for BIR-1g than the GeoReM-preferred values. The systematically lower Na_2O and P_2O_5 of USGS glasses obtained in this study relative to GeoReM-preferred values is due to the use of VG 2 as the major element standard. Replicate analyses (n = 14) of 15 trace elements whose abundances were previously not well determined in the USGS glasses are also given in Table S1. Analytical uncertainty is less than 10% (1σ) for most of the trace elements analyzed in USGS glasses in this study and is 3% (1σ) for Ga and Ge. The analytical uncertainty is larger (>20%, 1σ) for elements that are extremely depleted (ppb level; e.g., Ag, Re, and Bi) in natural basalts and for elements with strong *memory effect* (e.g., Li, Cs) in the instrument.

Long-term data precision was assessed by examining the reproducibility of multiple analyses of the VG 2 and USGS glasses, which were run routinely with MORB glasses as reference materials. The analytical precision, assessed by the replicate measurements of USGS glasses, is comparable with that assessed by the replicate measurements of VG 2. While VG 2 was used as the calibration material for most major elements, it was treated as an unknown for FeO_T, MnO, and trace elements in this study. The uncertainties of trace element analyses were obtained by calculating the 1σ standard deviation of the 23 replicate analyses of VG 2 (Table S1), with each analysis being the daily mean of five replicate spots. The analytical precision is better than 6% (1σ) for most of the elements analyzed in VG 2, and is 3% (1σ) for Ge, particularly. The analyses of Li, Be, B, Ag, Sb, Cd, Cs, Re, and Bi are less precise (>20%, 1σ), due to their low abundances in natural basalts or high blank corrections during analysis (e.g., Li and Cs). Cesium abundances from only two localities are shown in the figures.

Another indication of the precision is derived from the analyses of a set of 32 MORB samples from a single chemical group (A 15.41 Na1) from north of 15°20 FZ identified on the basis of major elements (Melson et al., 2002). The highly incompatible element abundances for these 32 samples (Table S1) agree within the analytical precisions obtained from replicate analyses of VG 2 (Table S1), confirming that MORB flows identified on the basis of major elements are also homogeneous in trace elements.

Accuracy of the analytical method was assessed by the comparison of the analyses of MPI-DING glasses obtained in this study with their GeoReM values (Table S1). For seven MPI-DING glasses (GOR-128G, GOR-132G, ATHO-G, ML3B-G, KL2-G, TI-G, and StHs6/80-G) analyzed in this study, the percentage deviation

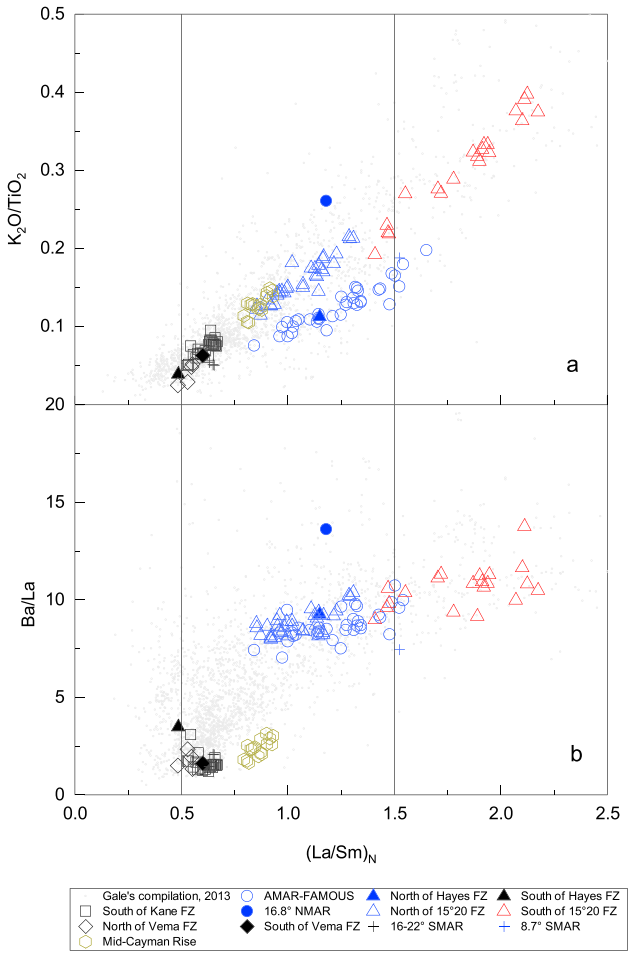

Figure 2. Correlations of K_2O/TiO_2 (a) and Ba/La (b) against $(La/Sm)_N$ of MORBs analyzed in this study, along with the MORB data compiled in Gale et al. (2013). $(La/Sm)_N$ is the primitive mantle (PM)-normalized La/Sm ratio. The PM composition is taken from McDonough and Sun (1995). MORB samples analyzed in this study were classified into depleted (D)-MORB with $(La/Sm)_N < 0.8$ and enriched (E)-MORB with $(La/Sm)_N > 1.5$ following Gale et al. (2013). In this study, MORBs with (La/Sm) N between 0.8–1.5 were considered as normal (N)-MORBs, which have narrower compositional spectrum than that of N-MORB used in Gale et al. (2013) referring all MORB compositions along the global ridge system excluding back-arc spreading center. Samples that plotted on the constant $(La/Sm)_N$ lines of 0.8 and 1.5 were grouped with the majority of samples from that ridge segment. Although mid-Cayman rise samples are plotted in N-MORB segment along the trend of K_2O/TiO_2 versus $(La/Sm)_N$ (a), they have Ba/La ratios that are distinctively lower than Ba/La in N- and E-MORBs (b) and therefore are classified as a separate group. D = depleted; N = normal; E = enriched; MORB = mid-oceanic ridge basalt; AMAR-FAMOUS = Valley and the French-American Mid-Ocean Undersea Study; NMAR = North Mid-Atlantic Ridge; SMAR = South Mid-Atlantic Ridge.

of the compositions determined in this study from the GeoReM values are a few percent for most of the elements. These deviations are larger for some chalcophile and siderophile elements (e.g., Ge, Ag, Sn, Sb, In, Cd, and Re) whose concentrations are given only as information values in GeoReM, and for some elements that are extremely depleted (e.g., P_2O_5 in ATHO-G; Th and U in GOR-132G).

Nielsen and Lee (2013) reported Tl abundances in the three USGS glasses. The Tl concentrations of the three USGS glasses measured in this study agree within errors of the values reported by Nielsen and Lee (2013; Table S1).

3.2. Lithophile Trace Elements

While some workers have debated the value of compositional groupings (Jenner & O'Neill, 2012), for consistency with the larger MORB community (Gale et al., 2013) MORBs analyzed in this study were classified into depleted (D)-MORB, normal (N)-MORB, and enriched (E)-MORB based on the ratio of (La/Sm) normalized to primitive mantle (PM), marked as $(La/Sm)_N$ (Figure 2). Following Gale et al. (2013), MORBs with $(La/Sm)_N < 0.8$ are considered as depleted while with $(La/Sm)_N > 1.5$ are considered as enriched in this study. However, Gale et al. (2013) considered N-MORB to be any kind of MORB along the global ridge system excluding basalts from back-arc spreading centers, while here we restrict the term exclusively to MORBs that are neither D-MORB nor E-MORB. A couple of additional adjustments were made as follows. A few samples from AMAR-FAMOUS with $(La/Sm)_N$ slightly below 0.8 (Figure 2) were considered as N-MORBs since their Ba/La ratios are significantly higher than Ba/La of D-MORB (Figure 2b). AMAR-FAMOUS samples with $(La/Sm)_N$ of 1.50 to 1.55 (Figure 2) were also grouped as N-MORBs with the majority of samples from this ridge segment. Although MCR MORBs have $(La/Sm)_N$ and K_2O/TiO_2 ratios of N-MORBs (Figure 2a), their Ba/La are distinctly lower than that of N- and E-MORBs and are comparable to that of D-MORB (Figure 2b). Therefore, MCR MORBs were treated as a distinct group in this study. The grouping used in this study for MORB is shown by a color-coded scheme in Figure 2 that is used consistently throughout this manuscript.

PM-normalized spider diagrams of MORBs are shown in Figure 3 by locality, along with the mean compositions of D- and E-MORBs from Gale et al. (2013) for comparison. The trace elemental patterns of the D-MORBs analyzed in this study are similar to that of the global average D-MORB (Gale et al., 2013) but are more depleted in highly incompatible elements such as Rb, Ba (Figures 3b and 3e). All E-MORBs analyzed in this study are from one ridge segment of south of the 15°20 FZ (Figure 3d), showing the trace elemental pattern that is consistent with the global E-MORBs from Gale et al. (2013). N-MORBs (Figures 3a and 3c) defined in this study are plotted between the global averages of D- and E-MORBs of Gale et al. (2013). The effect of fractional crystallization on MORB compositions results in parallel patterns of the spider diagrams of densely sampled MORB suites, including AMAR-FAMOUS (Figure 3a), South of Kane FZ (Figure 3b), north (Figure 3c) and south (Figure 3d) of 15°20 FZ, and Mid-Cayman Rise (Figure 3f).

To better observe the systematics of D-, N-, and E-MORBs, trace element ratios are plotted against $(La/Sm)_N$ as an index of source fertility in Figures 4 and 5, together with MORB data compiled in Gale et al. (2013) for comparison. The average values of these ratios of D-, N-, and E-MORBs determined in this study are given in Table S1.

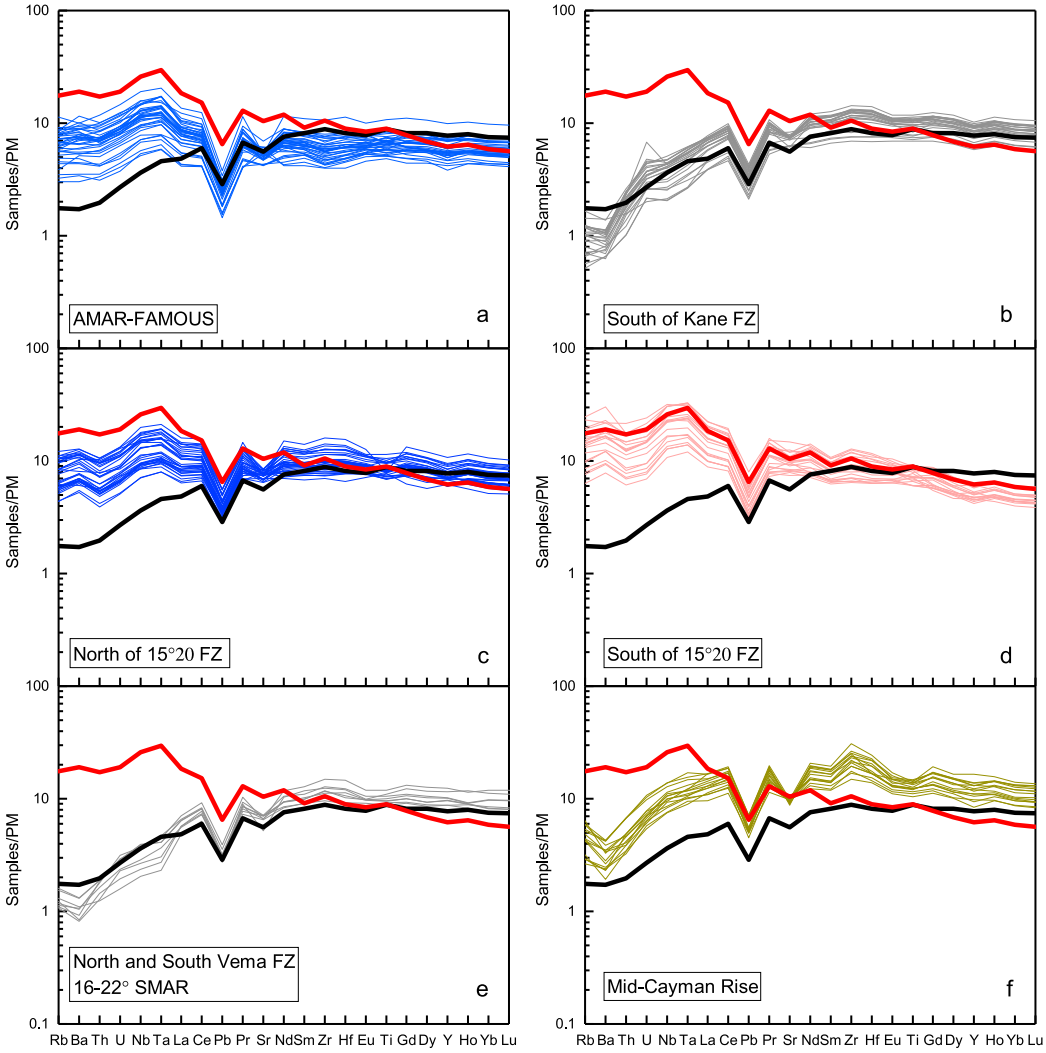

Figure 3. (a–f) PM-normalized spider diagram of MORBs analyzed in this study, along with the mean compositions of global D-MORB and E-MORB from Gale et al. (2013). PM composition is from McDonough and Sun (1995). PM = primitive matle; D = depleted; N = normal; E = enriched; MORB = mid-oceanic ridge basalt; AMAR-FAMOUS = Valley and the French-American Mid-Ocean Undersea Study; SMAR = South Mid-Atlantic Ridge.

Figures 4 and 5 show that $(La/Sm)_N$ and other trace lithophile ratios of regional MORBs analyzed in this study cover the range of variation of these ratios observed in global MORB (Gale et al., 2013). The ratio of two highly incompatible elements should be a planetary constant if the elements are of similar incompatibility (Hofmann, 1988), but small differences in compatibilities of some elemental pairs are revealed based on our MORB data. For example, the Th/U ratio is constant in all but the D-MORBs and MCR basalts (Figure 4a), where the lower ratio implies source depletion of the more incompatible Th. A similar effect is seen in Ba/La (Figure 4i), and a lesser effect is seen in the Nb/U (Figure 4b) and Ba/Th (Figure 4h) ratios. The K/Rb ratio (Figure 4d) illustrates the opposite compatibility relationship with K being higher in more depleted sources than Rb. A lesser effect is seen in K/U (Figure 4c). Some of the ratios for the more incompatible element-enriched MORBs agree well with those of PM (e.g., Th/U, Nb/U, K/Rb, Ba/Rb, Ba/Th, and Ba/La), but the Cs/Rb ratio is a factor of 2 lower in MORB than in PM (Figure 4e), which may require reevaluation of the PM Cs/Rb ratio. Ratios of Rb/Sr of E-MORBs and most of N-MORBs are above, while those in D-MORBs are below the PM value (Figure 4f).

Refractory element ratios plot close to the chondritic values. Interestingly, the $(Sm/Nd)_N$ and $(Gd/Yb)_N$ ratios of D-MORBs and MCR MORBs form a parallel trend to that of N- and E-MORBs (Figures 5a and 5d). In Figure 5e,

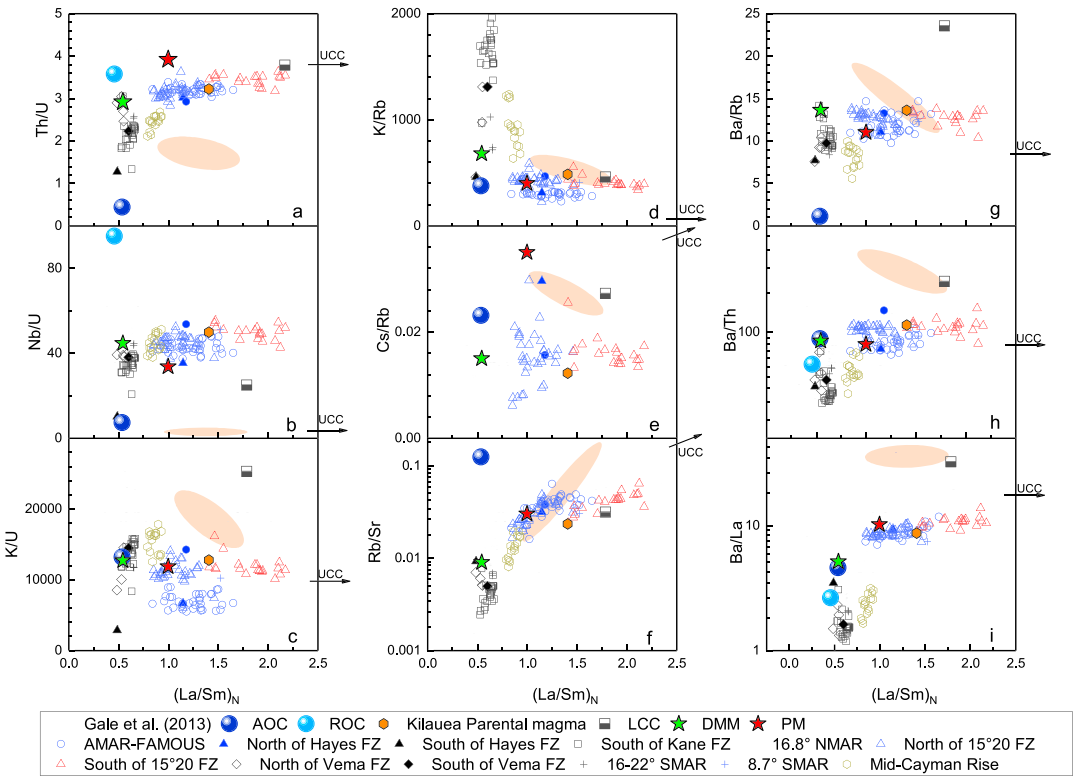

Figure 4. (a–i): Correlations of lithophile trace elements ratios against $(La/Sm)_N$ of MORBs analyzed in this study and MORBs compiled in Gale et al. (2013). The compositions of several geochemical reservoirs shown in this figure are as follows: Altered oceanic crust (AOC) of ODP site 801 (Kelley et al., 2003); estimated composition of the recycled oceanic crust (ROC) that has undergone the chemical modification through subduction (Stracke & Bourdon, 2009); Kilauea parental magma from Norman and Garcia (1999), lower continental crust (LCC) and upper continental crust (UCC) of Taylor and McLennan (1995) in plot (a) and of Rudnick and Gao (2003) in other plots; depleted MORB mantle (DMM) from Salters and Stracke (2004) and primitive mantle (PM) from McDonough and Sun (1995). Orange field shows the composition of Manus Basin arc lava from Jenner et al. (2012). MORB = mid-oceanic ridge basalt; AMAR-FAMOUS = Valley and the French-American Mid-Ocean Undersea Study.

the Zr/Hf ratios of MAR D-, N-, and E-MORBs are identical to the chondritic value (34.3, Münker et al., 2003), except for glasses from the AMAR-FAMOUS region that plot 0–10% below the chondritic value. The Nb/Ta ratios (Figure 5f) for D-MORBs are ~10% lower than those of N- and E-MORBs, which in turn are ~20% lower than the chondritic value (19.9, Münker et al., 2003).

Although MCR MORBs have $(La/Sm)_N$ of 0.8–0.9 higher than the D-MORB range of $(La/Sm)_N < 0.8$ (Gale et al., 2013), they are comparable with D-MORB in many trace element ratios, such as Th/U (Figure 4a), Ba/Rb (Figure 4g), and Ba/Th (Figure 4h), so that their high $(La/Sm)_N$ likely represents a lower degree of melting rather than an enriched source. Accordingly, plots of the ratios of $(Hf/Sm)_N$ (Figure 5b) and $(Zr/Hf)_N$ (Figure 5e) show that MCR basalts have Zr > Hf > Sm, which may indicate the small differences of the compatibilities of D (Zr) < D (Hf) < D (Sm) that can only be revealed by lower degree melts than typical MORBs. AMAR-FAMOUS N-MORBs have distinctly lower K/U (Figure 4c), K/Rb (Figure 4d), Ba/Th (Figure 4h), $(Zr/Hf)_N$ (Figure 5e), and $(Gd/Yb)_N$ (Figure 5d) relative to those ratios in other MAR N-MORBs analyzed in this study.

3.3. Siderophile and Calcophile Element

We first compared the siderophile and chalcophile data from this study with that from literature. (*As*): Arsenic abundances range from 50 to 400 ppb for 313 analyses of MORB glasses, but the majority of glasses have 100–200 ppb As. The range for As is smaller than that reported by Jenner and O'Neill (2012), who noted a range from 0 to >1 ppm for 299 MORB analyses, while Kelley et al. (2013) did not report As abundances. (*Mo*): Molybdenum abundances range from 200 to 1,000 ppb for 319 analyses of MORB glasses, smaller than the range (200–3,000 ppb) reported in Jenner and O'Neill (2012) for 532 MORB analyses and the range (60–3,000 ppb) reported in Kelley et al. (2013) for 573 MORBs. (*Ag*): Silver abundances range from 10 to

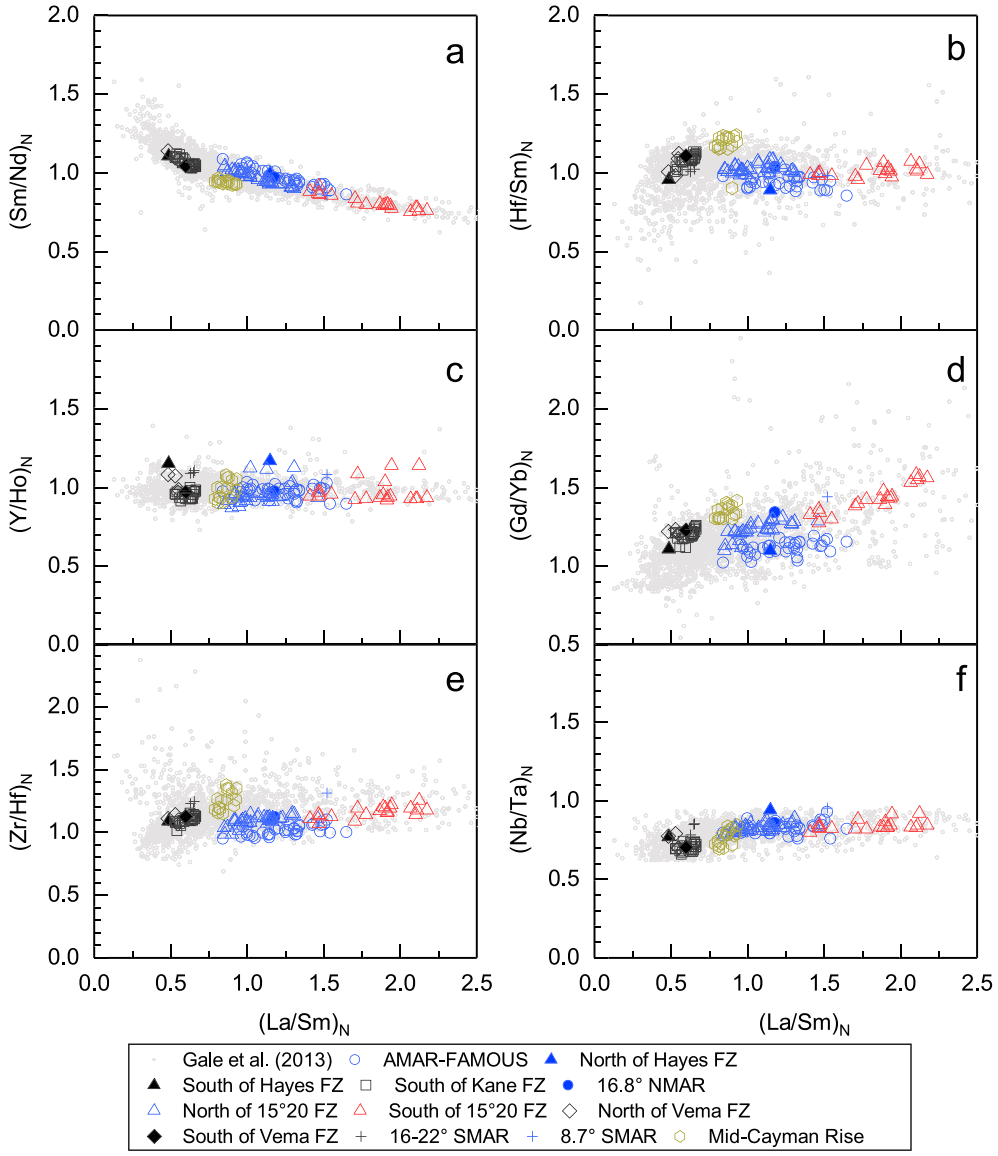

Figure 5. (a–f) Correlations of chondrite-normalized lithophile trace element ratios against $(La/Sm)_N$ of MORBs analyzed in this study and MORBs compiled in Gale et al. (2013) chondritic values are taken from Anders and Grevesse (1989) except for Nb/ta and Zr/Hf that are from Münker et al. (2003). MORB = mid-oceanic ridge basalt; AMAR-FAMOUS = Valley and the French-American Mid-Ocean Undersea Study; FZ = fracture zones; NMAR = North Mid-Atlantic Ridge; SMAR = South Mid-Atlantic Ridge.

50 ppb for 319 analyses of MORB glasses, similar to the range in Ag abundances noted by Hertogen et al. (1980) for seven MORB analyses and by Jenner and O'Neill (2012) for 307 MORB analyses. (*Cd*): Cadmium abundances range from 50 to 200 ppb for 319 analyses of MORB glasses, larger than the range reported for seven MORBs (50–150 ppb) by Hertogen et al. (1980), similar to the range reported in Jenner and O'Neill (2012) for 568 analyses (100–240 ppb) but smaller than that reported in Kelley et al. (2013) for 573 analyses (6–500 ppb). (*In*): Indium abundances in MORB glasses from this study (50–100 ppb) overlaps that of Hertogen et al. (1980) but smaller than the range (50–150 ppb) of Jenner and O'Neill (2012), with the MCR glasses having the highest In abundances. (*Sn*): Tin abundances range from 0.4 to 2.4 ppm in 319 MORB glasses, similar to the range observed in 568 MORB analyses by Jenner and O'Neill (2012) but smaller than the range (0.04–4 ppm) of Kelley et al. (2013), with the MCR glasses exhibiting the highest Sn contents (1.5–2.4 ppm). (*Sb*): Antimony abundances range from 20 to 140 ppb in 319 MORB glasses from

this study, with the highest values (>100 ppb) in the MCR glasses, compared with 2–74 ppb (Hertogen et al., 1980), 4–40 ppb in 250 analyses from Jenner and O'Neill (2012), and 10–200 ppb in 562 analyses from Kelley et al. (2013). (*W*): Tungsten abundances range from 10 to 250 ppb in 319 MORB glasses from this study, which are narrower compared with the ICP-MS analyses from three previous studies, including 6–555 ppb in 50 MORBs from Arevalo and McDonough (2008), 3–600 ppb in 548 MORBs from Jenner and O'Neill (2012), and 50–1500 ppb in 572 MORBs from Kelley et al. (2013), but comparable with an isotope dilution data set of MORBs (5–220 ppb) from König et al. (2011). (*Re*): Rhenium abundances range from <0.1 to 2 ppb in glasses from this study, with the average of 1.33 ± 0.52 (1σ), a range similar to that obtained by Hertogen et al. (1980), Hauri and Hart (1997), Schiano et al. (1997), Sun et al. (2003), Escrig et al. (2005), and Schilling and Kingsley (2017). Jenner and O'Neill (2012) reported 154 analyses of Re in MORBs with an average of 0.7 ± 0.6 ppb, with most of the analyses ranging from 0.1 to 0.8 ppb, systematically lower than that obtained in this study They applied an interference correction for TmO+ that was not applied here after we determined that such a correction would be negligible. (*Tl*): Thallium abundances range from 3 to 35 ppb in 319 MORB glasses from this study, comparable with that from 3 to 30 ppb in 97 MORB analyses from Nielsen et al. (2014) and from 2 to 50 ppb in 531 MORB analyses from Jenner and O'Neill (2012), and consistent with the range of 7–22 ppb found by Hertogen et al. (1980). The data set from Kelley et al. (2013) reported Tl contents in some MORB samples at the ppm level, but we did not observe such Tl enrichment in any of the glasses studied. (*Pb*): Lead abundances range from 0.2 to 1.2 ppm in 319 MORB glasses from this study, similar to 0.1–1.9 ppm of 568 MORB analyses from Jenner and O'Neill (2012) and 0.1–6.2 ppm of 573 MORBs analyzed by Kelley et al. (2013). MCR MORBs have Pb contents (0.6–1.1 ppm) as high as the E-MORBs analyzed in this study. N-MORBs from AMAR-FAMOUS have lower Pb (0.2–0.5 ppm) relative to that (0.4–0.7 ppm) of other N-MORBs from our study. (*Bi*): Bismuth abundances range from 6 to 15 ppb in 319 MORB glasses, with an average of 10 ± 3 ppb Bi. For comparison, Hertogen et al. (1980) reported 6–9 ppb Bi in seven MORBs, and Jenner and O'Neill (2012) reported a lower range of 4–15 ppb of Bi in 529 MORB analyses. It is disheartening that 23 analyses of VG 2 yielded a range from 3 to 24 ppb Bi, with an average of 13 ± 5 ppb, but reproducibility on BCR-2g was better, 55 ± 6 ppb Bi, compared with ~50 ppb given in GeoREM.

Ratios of chalcophile and siderophile elements to lithophile elements with similar compatibilities were then compared. Ratios of As/Ce, Tl/Ce, Pb/Ce, In/Y, Sn/Sm, Sb/Sm, Mo/La, Cd/Dy, Ag/Cu, W/Ba, Bi/Dy, and Re/Yb plotted against $(La/Sm)_N$ in Figure 6, along with the recommended *canonical* values and literature data if available.

4. Discussion

4.1. Lithophile Trace Element Systematics of MORBs

MORB glass compositions have been modified by fractional crystallization processes prior to eruption on the oceanic floor (e.g., Coogan & O'Hara, 2015; Grove & Bryan, 1983; Klein & Langmuir, 1987). Incompatible trace element ratios have been widely employed to examine variations in mantle source characteristics since the partitioning of these elements into both mantle and crustal mineral assemblages is minimal (Hofmann, 1988). The chemical information contained in incompatible element ratios is regarded to be dominated by mantle source depletion and enrichment processes with only minimal effects coming from partial melting or magma chamber processing that occur prior to eruption of MORB lavas. Some workers have questioned this long-held notion arguing that magma chamber processes affect all but the most highly incompatible element ratios (e.g., Coogan & O'Hara, 2015; Lissenberg & MacLeod, 2016; O'Neill & Jenner, 2012, 2016). Reactive porous flow in cumulate piles within MORB magma chambers potentially creates elemental fractionations among the least incompatible elements that differ from fractional crystallization due to buffering of the Mg# by olivine (Lissenberg & MacLeod, 2016). The role of diffusive elemental fractionation in cumulate piles has been invoked by Coogan and O'Hara (2015), but zoning profiles of clinopyroxene in ODP 735B gabbros does not support a role for diffusive fractionation (Lissenberg & MacLeod, 2016) The reactive porous flow model proposed by Lissenberg and MacLeod (2016) invoked zone refining for creating incompatible element enrichments in excess of fractional crystallization involving melt exchange with 4–8 equivalent volumes of pyroxene-rich cumulates. To assess the effect of magma chamber processes on incompatible lithophile elemental ratios, Figure 7 compares ratios of elements differing in compatibility by about an order of magnitude ranging from highly incompatible to less incompatible: Ba/La (Figure 7a), Rb/Sr (Figure 7b), $(La/Yb)_N$

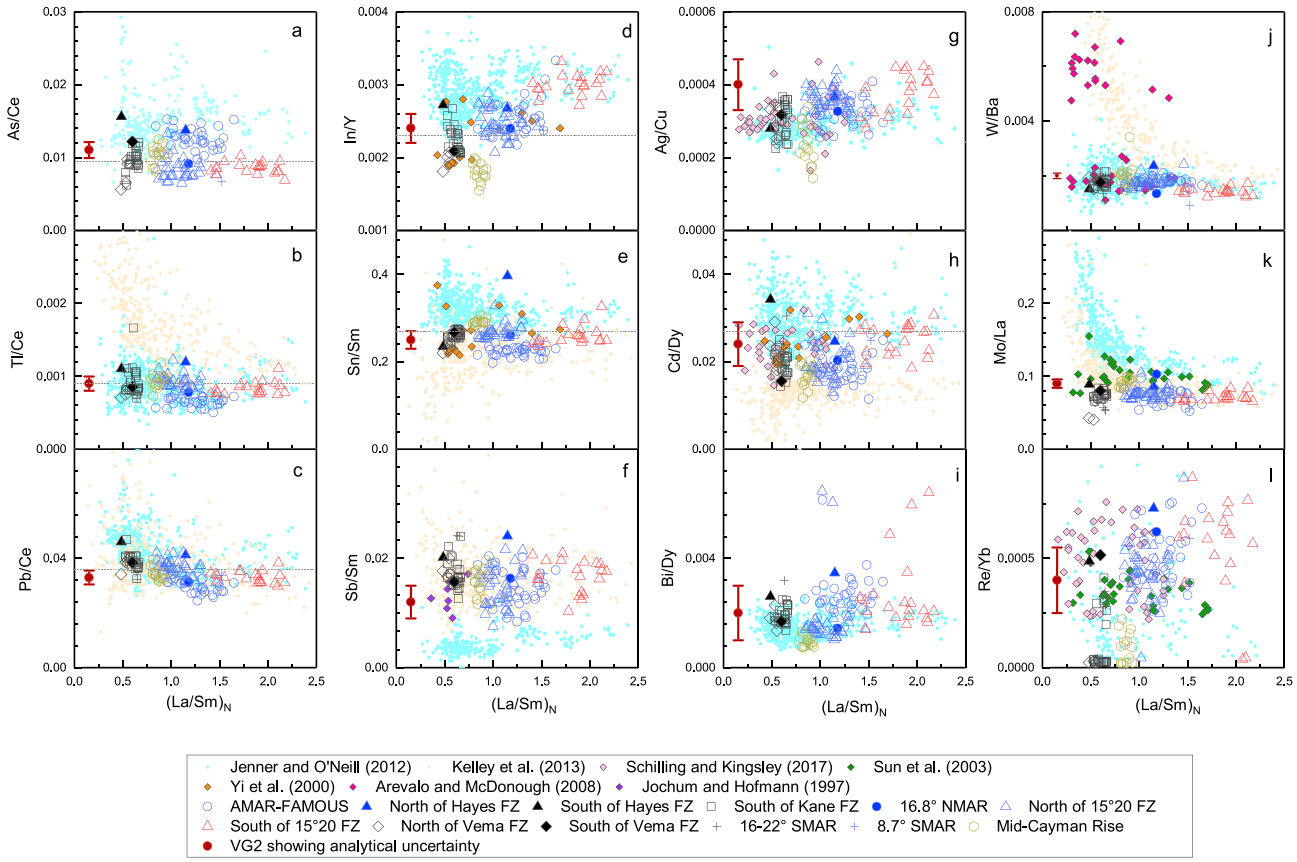

Figure 6. (a–l): Correlations of ratios of chalcophile and siderophile elements to lithophile elements with similar compatibilities against $(La/Sm)_N$ of MORBs analyzed in this study. Literature data are shown for comparison if available. The mantle ratios recommended by prior studies are shown as black lines for the purpose of references, which are in (a) As/Ce = 0.01 (Sims et al., 1990), (b) Tl/Ce = 0.0009 (Nielsen et al., 2014), (c) Pb/Ce = 0.036 (Newsom et al., 1986), (d) in/Y = 0.003 (Yi et al., 2000), (e) Sn/Sm = 0.32 (Jochum et al., 1993), (h) Cd/Dy = 0.027 (Yi et al., 2000). VG 2 with error bars showing the analytical uncertainties were plotted at low $(La/Sm)_N$ = 0.2 to avoid obscuring the data points. MORB = mid-oceanic ridge basalt; AMAR-FAMOUS = Valley and the French-American Mid-Ocean Undersea Study; FZ = fracture zones; NMAR = North Mid-Atlantic Ridge; SMAR = South Mid-Atlantic Ridge.

(Figure 7c), and La/Zr (Figure 7d). In Figure 7, Mg# has been used as the index of fractionation, with the standard assumption that the $Fe^{+3}/\sum Fe$ ratio is 0.15, justified by recent experimental work (Zhang et al., 2018).

MORB glass data were selected from this study and from Jenner and O'Neill (2012). To better examine the effects of magma chamber processes, glasses were grouped according to ridge segments that were assigned based on the discontinuities at fracture zones along MAR and EPR using GeoMap APP (http://www.geomapapp.org). The MORB glasses were filtered using the following criteria and plotted in Figure 7 by location. To obtain sufficient range of Mg# to define the fractionation trends of MORB lava flows, only segments that were densely sampled ($N \geq 8$) with MORBs covering an Mg# range ≥5 were plotted. The average compositions of 137 MORB lava flows from five ridge segments from the NMAR were selected from this study, and the compositions of 260 MORB analyses from 13 ridge segments from both MAR and EPR taken from Jenner and O'Neill (2012) met the criteria (Figure 7). MORBs from Jenner and O'Neill (2012) were assigned D-, N-, or E-MORB following the same criteria Gale et al. (2013) laid out for glasses from this study. Galapagos spreading center MORBs analyzed in Jenner and O'Neill (2012) are also shown in Figure 7 as four groups (K11, K12, K17, and K28). Glasses from the Blanco Trough, which may be influenced by the Juan de Fuca hotspot (Courtillot et al., 2003), contain D-, N-, and E-MORBs that were plotted separately in Figure 7.

Following Lissenberg and MacLeod (2016), we calculated the effects of zone refining in a crustal magma chamber with mineral abundances from Lissenberg and MacLeod (2016) and partition coefficients from Bédard (2001). Because of the high fraction of plagioclase in the models of Lissenberg and MacLeod (2016), the Ba/La ratio is predicted to decrease by factors of 2–3 with increasing zone refining, contrary to

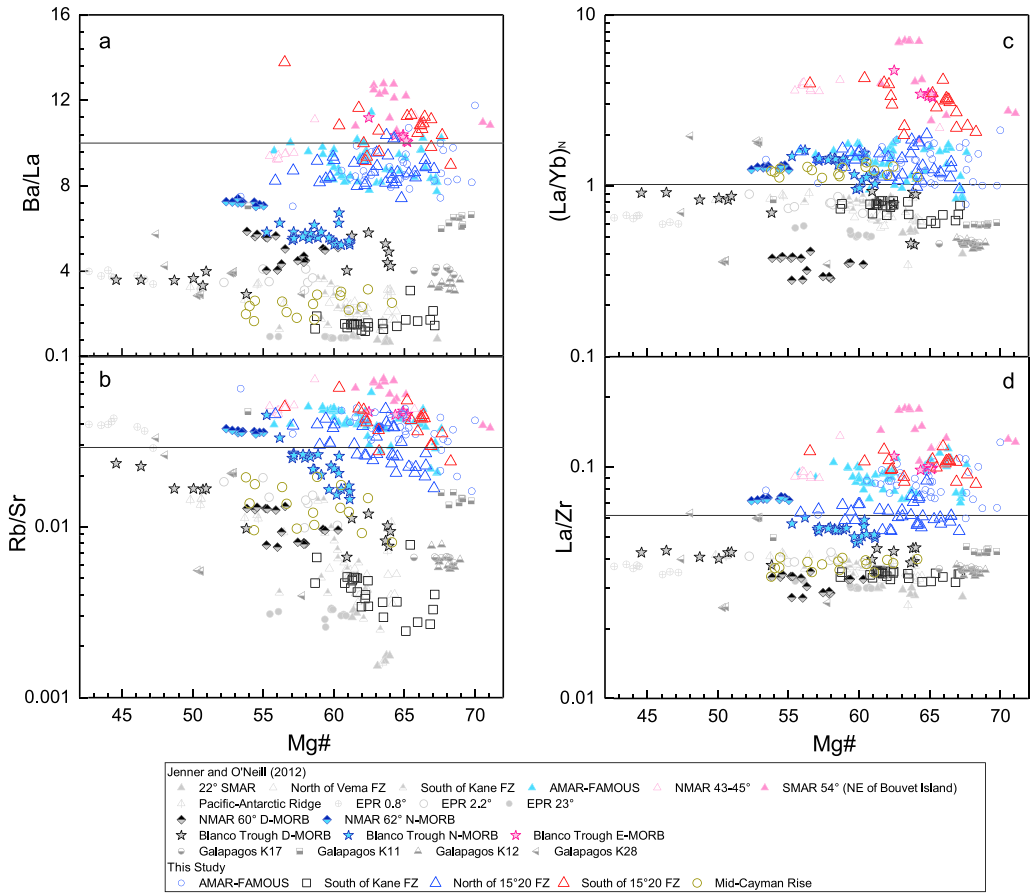

Figure 7. Plots of ratios of Ba/La (a), Rb/Sr (b), C1-normalized La/Yb (c), and La/Zr (d) against the fractional crystallization index Mg# [Mg# = 100*Mg/(0.85*Fe + mg)] of MORB analyses from this study and Jenner and O'Neill (2012). MORB data were grouped by ridge segments (see text) and color coded for quick recognition as, black: D-MORB; blue: N-MORB, and red: E-MORB. Straight line in each plot indicates the PM value from McDonough and Sun (1995). MORB = mid-oceanic ridge basalt; AMAR-FAMOUS = Valley and the French-American Mid-Ocean Undersea Study; FZ = fracture zones; NMAR = North Mid-Atlantic Ridge; SMAR = South Mid-Atlantic Ridge.

what is observed for the variations within individual segments (Figure 7a). Thus, zone refining cannot explain the Ba-enrichment of E-MORB compared to N- and D-MORB observed in Figure 7a.

Since Rb is much more incompatible than Sr, Rb/Sr ratios of MORB segments shown in Figure 7c are anticorrelated with Mg#. The systematics among D-, N-, and E-MORBs observed for Ba/La ratios (Figure 7b) are also observed for Rb/Sr (Figure 7c), which is that D-MORBs, except those from the Galapagos spreading center and Blanco Trough, are systematically lower in Rb/Sr ratios relative to that of N- and E-MORBs. The zone refining model discussed above predicts that Rb/Sr should increase by factors of 3–5, which is less than what is observed probably due to choices of partition coefficients.

The ratios of $(La/Yb)_N$ remain nearly constant along most MORB segments shown in Figure 7c. The $(La/Yb)_N$ ratio systematically increases from D-MORB to N-MORB to E-MORB. E-MORBs from the Blanco Trough do not form a continuum with N-MORBs, and the most fractionated D-MORBs from the Blanco Trough (Mg# < 55) have $(La/Yb)_N$ lower than those of N-MORBs. The zone refining model discussed above predicts an increase of 30–70% in the $(La/Yb)_N$ ratio of an intercumulus liquid, that is, variations that are comparable to those observed within a single segment, and cannot explain the segment-to-segment variations or the differences between D- and E-MORBs (Figure 7c). Van Orman et al. (2001) showed that La diffuses more than an order of magnitude more slowly into clinopyroxene crystals than Yb, and trivalent REE are slow diffusers compared with Fe-Mg exchange. A simple prediction for the deviation of the composition of an evolving intercumulus liquid within a MORB magma chamber from fractional crystallization is that the faster diffusive transport of

Fe-Mg versus La-Yb would manifest itself in La becoming more incompatible than predicted at a given Mg#. Mixing of intercumulus liquid into the magma chamber (e.g., Coogan & O'Hara, 2015) would then produce mixed liquids that exhibit higher (La/Yb) N at a given Mg# than predicted by fractional crystallization. One might also expect that the longer magma resides in the magma chamber the more intercumulus liquid is mixed into it. Thus, at lower Mg#s a larger range of $(La/Yb)_N$ would be expected from models involving replenishment, fractionation, mixing, and tapping relative to simple fractional crystallization of magma. This is not observed in the Blanco Trough MORBs, where the largest range in $(La/Yb)_N$ is observed at the highest Mg#s. The effect is similar for the La/Zr ratio (Figure 7d), even though Zr is more compatible, and as a tetravalent cation Zr might be a slower diffuser than La resulting in reverse enrichments during crustal processes. No reverse enrichment is observed in La/Zr (Figure 7d). The systematic variation observed between D-, N-, and E-MORBs in four pairs of elements that vary significantly in their compatibility failed to be produced by crustal processes involving fractional crystallization or zone refining, with or without diffusive fractionation in the cumulate pile. Thus, Figure 7 shows that mantle heterogeneity is required to explain the distinct differences observed between D-, N-, and E-MORBs and that any effects associated with magma chamber processes are second order, or lower, effects.

Lithophile trace elements have been used to study source depletion and enrichment processes during MORB genesis (e.g., Langmuir et al., 1993; Niu & O'Hara, 2008) and the chemical (e.g., Donnelly et al., 2004; Sun & McDonough, 1989; Zindler et al., 1984) and mineralogical (e.g., Donnelly et al., 2004; Hémond et al., 2006; Stracke & Bourdon, 2009; Ulrich et al., 2012) heterogeneities of the MORB mantle. Crust-mantle differentiation as an igneous process would be expected to create a depleted mantle that is compositionally complementary to the continental crust (Hofmann, 1988). Recycling of subducted oceanic crust into the depleted mantle would be expected to enrich it in incompatible lithophile elements (Stracke & Bourdon, 2009). The origin of E-MORBs is classically thought to occur by ridge-plume interaction near hotspots (e.g., Schilling, 1973, 1985), but recent reexamination of global MORB compositions shows that E-MORBs constitute about 10% of ridge segments far from plumes (Gale et al., 2013). Thus, another process must be found to explain the enrichment observed in E-MORBs far from plume-affected ridge segments. Two major classes of hypotheses have been proposed both of which involve the role of recycled oceanic crust. Donnelly et al. (2004) proposed that the enrichment of depleted mantle occurred by the addition of low-degree (<1%) partial melts of recycled oceanic crust. In this model, the E-MORB source is an enriched peridotite but the lithophile element pattern is expected to inherit some of the chemical features of altered oceanic crust with or without a subduction filter imposed. Hémond et al. (2006) and Ulrich et al. (2012) argued that recycling of plume heads or OIBs into the mantle could create enrichments inherited by E-MORBs. Another possibility is that the suboceanic mantle contains abundant recycled oceanic crust, now garnet pyroxenites, the preferential partial melting of which produced the enriched lithophile element signatures of N- and E-MORBs (Hirschmann & Stolper, 1996; Sobolev et al., 2007). Correlations of $^{18}O/^{16}O$ and MORB enrichment index (e.g., La/Sm and K_2O/TiO_2; Eiler et al., 2000) and the heavier ?^{238}U of MORBs relative to the PM value (Andersen et al., 2015) have been taken as supporting evidence for the presence of recycled crustal material in the MORB mantle. Other sources of enriched mantle were proposed to be the lower portion of oceanic lithosphere hosting incompatible elements (Niu et al., 2002) or delaminated lithospheric mantle (Galer & O'Nions, 1986).

The systematics of lithophile trace elements of D-, N-, and E-MORBs from this study are shown in Figures 4 and 5, where lithophile elemental pairs are plotted against the ratio of $(La/Sm)_N$, an index of MORB source enrichment. The D-MORBs sampled in this study are compared with the global MORB data set of Gale et al. (2013), and it should be noted that the samples studied here include some of the most depleted MORBs relative to the global MORB data set and have narrow ranges of $(La/Sm)_N$ (0.55 ± 0.05) but show very broad ranges of incompatible-element ratios, such as Th/U, Nb/U, K/Rb, Rb/Sr, Ba/Rb, and Ba/La. Glasses from the MCR generally plot intermediate between D-MORB and N-MORB (Figure 4). Also shown on Figure 4 are estimates of PM, DMM, UCC, LCC, and estimates of altered oceanic crust (AOC; Kelley et al., 2003), recycled oceanic crust (ROC; Stracke & Bourdon, 2009) and Kilauea parental melt (KPM; Norman & Garcia, 1999). To assess possible arc signatures, the field defined by back-arc lavas from the Manus Basin (Jenner et al., 2012) is shown for comparison (Figure 4).

Since the ratio of $(La/Sm)_N$ is not fractionated significantly by melting or crystallization, melting a depleted MORB mantle, such as DMM with $(La/Sm)_N$ = 0.54 from Salters and Stracke (2004), yields the

observed $(La/Sm)_N$ ratios of the D-MORBs from this study. The main feature that emerges from each of the elemental ratio plots in Figure 4 is that N- and E-MORBs define a single ratio in Th/U, Nb/U, K/Rb, Ba/La, and Ba/Th, while D-MORBs are lower in all of these ratios, with the exception of K/Rb, where Rb is clearly more incompatible than K. The ranges of some ratios of elements of similar compatibility and similar fluid mobility, like K/U and Ba/Rb, of D-, N-, and E-MORBs overlap each other and that of most other terrestrial geochemical reservoirs (UCC, LCC, PM, DMM, and KPM), indicating that whatever process caused the enrichment of N- and E-MORBs in these elements left no clues in these ratios. The ratios of Nb/U, Ba/La, Ba/Th, and Th/U are sensitive to the influence of slab dehydration fluids formed at ≤4 GPa (Kessel et al., 2005), since Ba and U are highly mobile in such fluids compared with Nb, La, and Th. N- and E-MORBs do not show clear signatures of fluid mobile element enrichment in Th/U, Nb/U, Ba/La, and Ba/Th, in contrast with the Manus back-arc basin lavas that show such enrichments (Figures 4a, 4b, 4h, and 4i). It is immediately obvious that fluid addition processes that would affect the fluid mobile elements (K, Rb, Cs, Ba, and U) have played no role in the enrichment of D-MORB mantle to form N- or E-MORB sources within the studied samples from the NMAR. However, LCC shows low Nb/U, and high Cs/Rb, Ba/Rb, Ba/La, and Ba/Th ratios indicative of fluid-mobile element enrichment during continental crust formation processes. Only the Th/U ratio of UCC or LCC does not show significant evidence of U mobility.

A simple expectation of recycled oceanic crust is that it is likely to be depleted in fluid mobile elements relative to MORB composition after passing through the subduction zone. For example, ROC has undergone some Rb, Ba, and U loss during modification through subduction zones (Stracke & Bourdon, 2009) and has lower Ba/La (2.7) but higher Nb/U (95) relative to those ratios in mean MORB (Ba/La = 5.6; Nb/U = 45 in Gale et al., 2013). Thus, entrainment of recycled crust into the depleted mantle should create enriched mantle sources that have either enrichments or depletion of these element ratios since the specific degree of the presubduction alteration of ROC is highly variable (Eisele et al., 2002; Hémond et al., 2006; Stracke et al., 2003). Thus, the MORB glasses studied here show no evidence of material involved in subduction zones playing a significant role in the enrichment of depleted mantle to form N- or E-MORB sources. These observations exclude recycled oceanic crust, recycled altered oceanic crust, recycled subarc or back-arc mantle, or recycled lithospheric mantle enriched by ancient subduction events from forming a significant portion of the sources of NMAR MORB. Low-degree partial melts of recycled oceanic crust should be expected to concentrate elemental signatures of alteration of the oceanic crust that would affect alkalis, Ba and U abundances and ratios of these elements to nonfluid mobile elements of similar compatibility (Th, Nb, La, etc.). Thus, the model proposed by Donnelly et al. (2004) would only work if the recycled oceanic crust has neither been altered at the ridge/seafloor nor gone through the subduction zone or otherwise it would be difficult to have mobile/nonmobile element ratios that reflect PM values in the most enriched NMAR MORBs.

Continental crust, on the other hand, has higher Ba/La (22.8) but lower Nb/U (20; Rudnick & Gao, 2003) relative to the N- and E-MORB compositions. As shown in Figure 4, continental crust is not strictly complementary to D-MORB, since it has elemental fractionations in Cs/Rb that are not seen in any MORBs, but is similar to elemental signatures in the Manus Basin lavas from Jenner et al. (2012). Incidentally, the enriched elemental patterns of N- and E-MORBs are not unlike ratios observed in OIBs, for example, KPM plots on the trends defined by N- and E-MORBs.

4.2. Siderophile and Chalcophile to Lithophile Element Ratios in MORB

Siderophile and chalcophile element abundances in the mantle reflect equilibrium during core formation (Righter et al., 2015; Rubie et al., 2004), or subsequent reintroduction by late accretion processes (Ballhaus et al., 2013) or core–mantle exchange (Brandon, 1998). The MORB mantle likely represents a reservoir that has not interacted with the core after core formation, although Kelley et al. (2013) invoked core-mantle exchange in depleted MORBs. Thus, the siderophile and chalcophile element composition of the MORB mantle is key input parameter for models of core formation. Numerous studies have shown that ratios between elemental pairs such as As/Ce and Mo/Ce (Sims et al., 1990), Tl/Ce (Nielsen et al., 2014), Pb/Ce (Newsom et al., 1986), Sn/Sm (Jochum et al., 1993), Sb/Pr (Jochum & Hofmann, 1997), In/Y (Yi et al., 2000), Cd/Yb (Yi et al., 2000), W/U (Arevalo & McDonough, 2008), Rb/Tl (Hertogen et al., 1980), and Re/Yb (Sun et al., 2003) are nearly constant in oceanic basalts (cf. Jenner, 2017), due to the similarities of their compatibilities during partial melting and fractional crystallization. Although the *canonical* values recommended for these ratios have been extensively used to interpret MORB genesis and characterize the MORB mantle

sources in prior MORB studies (Arevalo & McDonough, 2008, 2010; Hofmann, 1988; Salters & Stracke, 2004; Sun & McDonough, 1989; Workman & Hart, 2005), the amount of data from which these ratios have been determined has been rather limited. In this study, we measured large numbers of MORB covering the global range in $(La/Sm)_N$ with significantly improved precision, providing an opportunity to reevaluate the MORB ratios for the following elements:

Arsenic: Our new data confirm that As abundances are best correlated with Ce abundances in oceanic basalts (Sims et al., 1990). The average MORB As/Ce ratio (0.010) determined in this study agrees with a global MORB + OIB estimate (0.0096) of Sims et al. (1990). The As/Ce ratios of MORB analyzed by Jenner and O'Neill (2012) show broader range than that of MORBs analyzed in this study (Figure 6a), particularly for D-MORBs, with an average As/Ce ratio (0.015) that is 50% higher than our estimate and that of Sims et al. (1990).

Molybdenum: Molybdenum has been considered to be similar to Ce in compatibility in MORB and OIB basalts (Newsom et al., 1986). However, our new data show that Mo/La ratios (Figure 6k) in all the MORBs from this study define a constant ratio (0.07 ± 0.01, 1σ) somewhat lower than that of Sun et al. (2003) but similar to that of Kelley et al. (2013) at all but the lowest $(La/Sm)_N$ ratios (Figure 6k). At the lowest $(La/Sm)_N$, the MORB data of Kelley et al. (2013) and of Jenner and O'Neill (2012) increase as if Mo were more compatible than La (Figure 6k). This is possibly due to an analytical artifact in those studies that is worst at low Mo contents, that is, constant Mo contents are observed at lowest Mo abundances. The Mo/La ratio in MORB analyses from Jenner and O'Neill (2012) are systematically higher than MORB from this study or any of the other published data sets available (Kelley et al., 2013; Sun et al., 2003) that sample all major ridges.

Silver: Unlike other chalcophile elements discussed here, Ag does not behave as an incompatible element in basaltic glasses and correlates inversely with moderately incompatible elements from Sm-Lu. Jenner (2017) showed that MORBs define a constant Cu/Ag ratio during fractionation. Schilling and Kingsley (2017) also found a constant Cu/Ag ratio in MORB from the Reykjanes Ridge. In Figure 6g, MORBs analyzed in this study, and those reported by Jenner and O'Neill (2012), define a constant Ag/Cu ratio (0.0003 ± 0.0001, 1σ) consistent with that observed by Jenner (2017) and Schilling and Kingsley (2017). A similar range of Ag/Cu (0.0003 ± 0.0001) was reported for mantle peridotites (Wang & Becker, 2015) indicating that this ratio is not fractionated by partial melting. The abundances of S are anticorrelated with Ag in MORB glasses from this study.

Cadmium: Although the analytical uncertainty (±23%, 1σ) of Cd/Dy ratio in MORBs obtained in this study is larger than that of other ratios examined here due to the analytical difficulties discussed earlier, Figure 6h shows that the Cd/Dy ratios (0.021 ± 0.005, 1σ) of MORBs determined in this study agrees with the Cd/Dy ratios obtained by isotope dilution analysis on a smaller group of MORBs (Schilling & Kingsley, 2017; Yi et al., 2000). MORB analyses of Jenner and O'Neill (2012) are systematically higher in Cd/Dy ratio, while those of Kelley et al. (2013) are systematically lower than the results of this study and of Yi et al. (2000) and Schilling and Kingsley (2017). Constant offset factors that adjust for different standards used in prior studies could bring the data sets of Jenner and O'Neill (2012) and Kelley et al. (2013) into agreement with the isotope dilution data and our LA-ICP-MS data.

Indium: In this study, In correlates well with Ti, Y and Tb-Yb and exhibits less correlation with Fe, Zn, and Ga, and correlates inversely with Mg#. The In/Y ratio (0.0025) in D- and N-MORBs measured in this study is in agreement with the isotope dilution analyses of Yi et al. (2000), while that of Jenner and O'Neill (2012) is higher (Figure 6d), but the In/Y ratios of the two data sets converge at higher $(La/Sm)_N$. Yi et al. (2000) pointed out that most OIBs have higher In/Y than that of MORBs due to the fact that Y is much more compatible in garnet than in spinel and clinopyroxene. Thus, a trace amount of garnet in the mantle residue will keep Y from entering basaltic melts and thus increase In/Y in the melts. This effect is seen in E-MORB samples analyzed in this study that exhibit an In/Y ratio of 0.003 (Figure 6d).

Tin: The best correlations of Sn are with Na, P, Zr, Sm, Eu, and Hf abundances in data from this study. Figure 6e shows the tight correlation between Sn and Sm in our data, similar to that in the data from Jenner and O'Neill (2012) and Kelley et al. (2013). The ratios of Sn/Sm (0.25 ± 0.03, 1σ) of MORBs analyzed in this study are consistent with the isotope dilution analyses from Yi et al. (2000) but lower than the PM values (0.32) given in the isotope dilution study of Jochum et al. (1993). Since Jochum et al. (1993) did not report Sm abundances, their data could not be shown in Figure 6e.

Antimony: Antimony has been argued to be similar to Pr in its compatibility (Jochum & Hofmann, 1997). Kelley et al. (2013) applied the Sb/Ce ratio to their data but did not obtain a constant ratio for all MORBs.

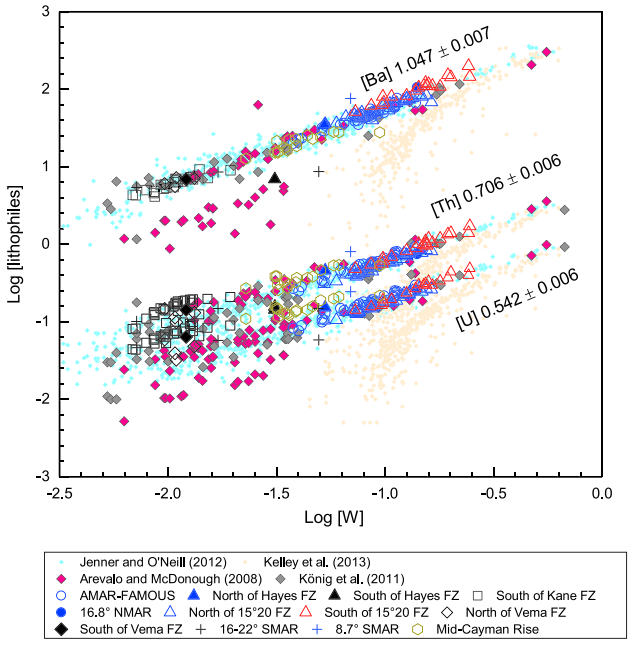

Figure 8. Log-log plot of the concentrations of Ba, Th, and U against that of W in MORBs analyzed in this study. Literature ICP-MS data from Arevalo and McDonough (2008), Jenner and O'Neill (2012), and Kelley et al. (2013), and isotope dilution data from König et al. (2011) are shown for comparison. Numbers shown next to the data trends are slopes calculated by performing York regression (York et al., 2004) of MORB data only from this study. MORB = mid-oceanic ridge basalt; ICP-MS = inductively coupled plasma mass spectrometry; AMAR-FAMOUS = Valley and the French-American Mid-Ocean Undersea Study; FZ = fracture zones; NMAR = North Mid-Atlantic Ridge; SMAR = South Mid-Atlantic Ridge.

Figure 6f shows that Sb/Sm remains nearly constant in D-, N-, and E-MORBs, indicating that Sb behaves more compatibly like Sm and Sn during magmatic processes. The isotope dilution data of Jochum and Hofmann (1997) have the same Sb/Sm ratios as our data and that of Kelley et al. (2013) but do not have a sufficient range of $(La/Sm)_N$ to appreciate the effect of melt depletion on the Sb/Sm ratios of MORBs. Figure 6f shows that Sb/Sm ratios of MORBs determined in this study (0.016 ± 0.005, 1σ) and in Kelley et al. (2013) are comparable with the isotope dilution data from Jochum and Hofmann (1997), while that ratio (0.005) from Jenner and O'Neill (2012) is lower, likely due to a standardization issue.

Tungsten: The geochemical behavior of W has been proposed to be most comparable to that of highly incompatible lithophile elements, such as Th, U, and Ba (Arevalo & McDonough, 2008; Jenner & O'Neill, 2012; Newsom et al., 1986, 1996; Sims et al., 1990). The ratio of W/Th of the bulk silicate Earth has been given as 0.20 ± 0.06 by Newsom et al. (1996). Arevalo and McDonough (2008) argued that W follows U during magmatic processes and estimated the ratio of W/U in the bulk Earth to be 0.65 ± 0.41. The issue of the compatibility of W in MORB is revisited in Figure 8. Following the approaches of Arevalo and McDonough (2008) and Nielsen et al. (2014), in Figure 8, log [Ba], log [Th], and log [U] are plotted against log [W] of MORBs analyzed in this study, along with LA-ICP-MS analyses from Arevalo and McDonough (2008) and Jenner and O'Neill (2012), solution ICP-MS analysis from Kelley et al. (2013), and isotope dilution ICP-MS data from König et al. (2011) for comparison. The correlations defined by data from this study and that of Jenner and O'Neill (2012), agree with the correlations obtained from the isotope dilution data of König et al. (2011). Data of Arevalo and McDonough (2008) agree with that of König et al. (2011) only at high abundances of Ba, Th and U, but exhibit higher W contents at low values of Ba, Th, and U (Figure 8). König et al. (2011) argued that the discrepancy between the LA-ICP-MS data (Arevalo & McDonough, 2008) and isotope dilution data (König et al., 2011) reflected instrumental problems in the LA-ICP-MS technique employed by Arevalo and McDonough (2008). The solution ICP-MS data of Kelley et al. (2013) exhibit systematically higher W as lithophile abundances become smaller, indicating analytical issues at lower W abundances.

Following Nielsen et al. (2014), the slopes of the correlations in Figure 8 were calculated applying York regressions (York et al., 2004) to MORB data from this study. The slope for log [W] and log [Ba] is 1.047 ± 0.007, while for log [W] and log [Th] is 0.706 ± 0.006 and for log [W] and log [U] is 0.542 ± 0.006, indicating W is more incompatible than U and Th but partitions most similarly to Ba during MORB magmatic differentiation. This finding is consistent with that of Jenner and O'Neill (2012), but at odds with that of Newsom et al. (1996) or that of Arevalo and McDonough (2008), although the latter conclusions are likely influenced by analytical problems at low W concentrations.

Rhenium: Rhenium has not been extensively analyzed in MORB studies, but was expected to behave as a moderately incompatible element that follows Yb during melting and differentiation (Hauri & Hart, 1997; Reisberg et al., 1993). Rhenium abundances obtained in this study are not precise enough to correlate with any elemental parameters, including S, Cu, or Yb. As shown in Figure 6l, the Re/Yb ratios in N- and E-MORBs obtained in this study are similar to the recent isotope dilution analyses from Schilling and Kingsley (2017). The MCR MORBs (<0.0002) and D-MORBs (mostly below the detection limit, 0.0001 ppm) in this study (Figure 6h) exhibit a systematically lower Re/Yb ratio relative to D-MORBs from Schilling and Kingsley (2017). The constant Re/Yb ratio (0.00028) of global MORB reported by Sun et al. (2003) has proven difficult to generalize to other MORB data sets (e.g., Figure 6l).

Thallium: The geochemical affinity of Tl with alkali metals makes it highly incompatible during magmatic process and depleted in residual mantle. Early work argued that Rb/Tl ratios in oceanic basalts were

constant at ~230 (Hertogen et al., 1980). Nielsen et al. (2014) found Tl to be less incompatible than Rb, due to partitioning into sulfides (Kiseeva & Wood, 2013), and showed that Tl has a constant ratio to Ce in MORBs. Our new data confirm that Rb/Tl ratio decreases from ~500 of E-MORBs to ~100 of D-MORBs, indicating that Tl is not as incompatible as Rb during mantle partial melting. Our data confirm that Tl has a constant ratio (0.0008 ± 0.0002, 1σ) to Ce in MORBs (Figure 6b), consistent with the value (Tl/Ce = 0.0009 ± 0.0002, 2σ) observed by Nielsen et al. (2014) and Jenner (2017).

Lead: Lead is well known to be similar to Ce in its compatibility and the mantle Pb/Ce has been proposed to be 0.036 by Newsom et al. (1986). Pb/Ce ratios (0.034 ± 0.004, 1σ) of MORBs analyzed in this study are comparable to that from Jenner and O'Neill (2012) and Kelley et al. (2013; Figure 6c).

Bismuth: Bi was rarely studied in MORB geochemistry (Hertogen et al., 1980), and the first extensive MORB data set was reported by Jenner and O'Neill (2012). The Bi abundances in MORB from this study overlap with that of Hertogen et al. (1980) and Jenner and O'Neill (2012) and do not correlate with indices of fractionation (Mg#) or source fertility $(La/Sm)_N$. By examining the partitioning of Bi relative to lithophile elements, we found that Bi weakly correlates with Dy (and other MREE) abundances. The Bi/Dy ratio in MORBs has been constrained to be 0.0002 ± 0.0001 (1σ) based on the MORB samples analyzed in this study. We obtained an average Bi/Dy ratio (0.00015 ± 0.00005, 1σ) of MORBs from the data of Jenner and O'Neill (2012), although Jenner (2017) found Bi is more compatible than Dy (Figure 6i).

Finally, estimates of the canonical ratios and their uncertainties derived from the present data set are summarized in Table S1. Because sample coverage is limited to the NMAR region, the ratios obtained are applicable to global values of the DM only where such ratios are not sensitive to regional chemical heterogeneities.

4.3. No Evidence for Core-Mantle Interaction in MORBs

Kelley et al. (2013) observed high ratios of Mo/Ce, Sb/Ce, and W/U ratios in the most depleted MORBs they analyzed. They interpreted this result as evidence of entrainment of small volumes (<1%) of outer core material in MORB sources, which would not affect the abundances of the lithophile elements used in the denominators. Particularly, they argued that really small contributions from the core were evident only in the most depleted basalts because those sources had very low W abundances. Results from this study show that there is no need to invoke excess siderophile element abundances in any of the MORB basalts studied here or by Kelley et al. (2013). For all three elements, we found that the choice of lithophile denominator strongly influences this conclusion. The tendency of such ratios in Kelley et al. (2013) to increase at low $(La/Sm)_N$ ratios is due to differences between the compatibility of Ce and that of Mo or Sb rather than any real enrichment of Sb or Mo in the MORB sources. When the Mo and Sb data of Kelley et al. (2013) are plotted relative to an element of similar compatibility (La or Sm), that effect disappears (Figures 6f and 6k). This is not true for W, where the data of Kelley et al. (2013) form ratios that increase at low concentrations of W (Figures 6j and 8). MORB data from this study, Jenner and O'Neill (2012) and from König et al. (2011) do not show this behavior. In this case, we suspect that Kelley et al. (2013) have either an interference or an uncorrected blank contribution to the W peak that cause these elemental abundances to become constant, while U abundances decrease at low $(La/Sm)_N$ ratios.

4.4. Mantle Differentiation of Chalcophile and Siderophile Elements

Melt extraction from the mantle is expected to deplete the incompatible chalcophile and siderophile elements, and enrich their abundances in the continental crust. In section 4.3 above, the relative compatibilities of chalcophile and siderophile elements have been considered. It has been known for a while that the Pb/Ce ratio in MORB and OIB is lower than that of the continental crust (Hofmann, 1988). Figure 9 shows the concentrations of chalcophile and siderophile elements normalized to PM (McDonough & Sun, 1995) for the averages of the D-, N-, and E-MORBs (this study), DMM (Salters & Stracke, 2004), and estimates of the composition of the continental crust (Hu & Gao, 2008; Rudnick & Gao, 2003). Also included are those key lithophile elements used in the ratios discussed above (section 4.3). To first order, the compositions of D-MORBs are consistent with elemental compatibility during melting of a depleted source (e.g., DMM, Salters & Stracke, 2004). In comparison with D-MORBs, E-MORBs are significantly more enriched (×10) in highly incompatible trace elements ($<D_{Nd}$) but are slightly more depleted (×0.1) in moderately incompatible ones ($>D_{Nd}$), possibly due to the existence of garnet in the source of E-MORBs. Imposed on the igneous compatibility trend are a series of anomalies that originate from either incorrect PM values (e.g., W, Cd, and Sn) used for normalization or from nonigneous processes (e.g., As, Tl, Pb, and Bi).

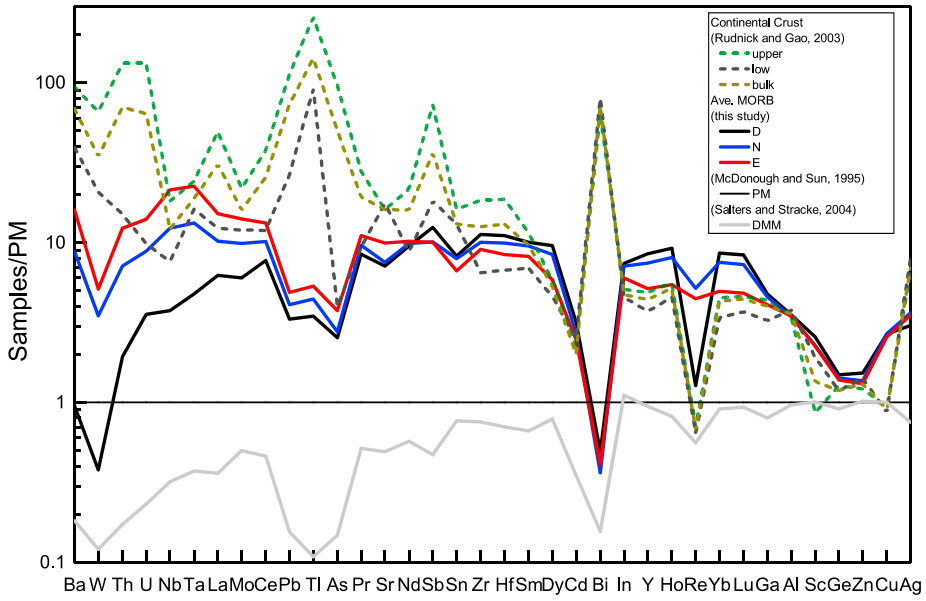

Figure 9. PM-normalized average compositions of chalcophile and siderophile elements in D-, N-, and E-MORBs analyzed in this study, the depleted MORB mantle from Salters and Stracke (2004) and the upper (U), lower (L), and bulk (B) continental crust (CC) from Rudnick and Gao (2003) and Hu and Gao (2008). The PM composition is taken from McDonough and Sun (1995). The key lithophile elements used as the constraints in the estimations of chalcophile and siderophile elements are also included. D = depleted; N = normal; E = enriched; MORB = mid-oceanic ridge basalt.

A systematic negative anomaly is seen in the W abundances in all MORBs and in the continental crustal compositions, from which it is inferred that the estimated W abundance (29 ppb) of PM (McDonough & Sun, 1995) is too high. This W anomaly disappears when using the revised PM abundance for W (12 ppb) of König et al. (2011). The abundance of Cd in both the continental crust and in the MORBs from this study and DMM (Salters & Stracke, 2004) shows a negative anomaly that is obscured by the adjacent Bi anomaly. The Cd anomaly appears to be an artifact of PM (McDonough & Sun, 1995) as well. The PM estimate for Cd was based on a single study of Cd in terrestrial basalts (Baedecker et al., 1971) from which mantle abundances were calculated assuming a constant Zn/Cd ratio, since Baedecker et al. (1971) did not report lithophile abundances for their samples. Since Cd is not depleted significantly by melt extraction, and does not appear to be concentrated in the continental crust by nonmagmatic processes, its abundance in the PM should be ~18 ppb (Yi et al., 2000), comparable to the 11–14 ppb estimated in DMM (Salters & Stracke, 2004), significantly lower than other estimates of PM: 35 ppb (Witt-Eickschen et al., 2009), 40 ppb (McDonough & Sun, 1995), 50 ppb (Lyubetskaya & Korenaga, 2007), and 60 ppb (Palme & O'Neill, 2003). Similarly, the slight negative anomaly of Sn in MORB from this study (Figure 9) disappears when substituting the PM values of Sn (91 ppb) from Witt-Eickschen et al. (2009) in place of the Sn content (130 ppb) from McDonough and Sun (1995). The PM values for As, Tl, Pb, and Bi undoubtedly need reexamination too, but because of the presence of large reciprocal anomalies in Figure 9, errors in PM values do not materially affect the outcome of the discussion below.

The elements As, Tl, Pb, and Bi are strongly depleted in MORBs and enriched in the continental crust (Figure 9), which is likely due to a nonmagmatic process discussed below. Estimates for Tl in the continental crust (Hu & Gao, 2008; Rudnick & Gao, 2003) are too high to balance the mantle abundances, and this issue will need to be reexamined. Estimates for Bi in the continental crust range from 60 to 280 ppb, with 180 ppb used as the nominal value (Rudnick & Gao, 2003). The higher number is based on an integration of the crust of China and is dominated by high-Bi analyses of the Interior North China craton (Gao et al., 1998). When analyses from this region are excluded, four other regions of China all exhibit 130–140 ppb Bi in the bulk continental crust, but we note that Hu and Gao (2008) obtained the same high Bi (230 ppb) as Gao et al. (1998) from a global set of upper crustal rocks. Heinrichs et al. (1980) obtained a lower estimate of Bi in the continental crust (85 ppb), about half the recommended value in Rudnick and

Gao (2003). The significantly higher enrichment of Bi over Dy in the continental crust is not in dispute regardless of the Bi estimate for the continental crust chosen (Gao et al., 1998; Heinrichs et al., 1980; Hu & Gao, 2008).

MORBs are generally regarded as partial melts derived from a residual mantle formed due to the extraction of the continental and oceanic crust (Hofmann, 1988). While oceanic crust is recycled back into the mantle, continental crust is stored as a distinct reservoir over geological time (e.g., Taylor & McLennan, 1995). Elements are transferred between the continental crust and mantle in several ways: (1) transfer by partial melts and magmatic intrusion into the crust; (2) transfer by hydrothermal processes to marine sediments followed by obduction of those sediments at trenches (Peucker-Ehrenbrink et al., 1994); (3) fluid transport in subduction zones (Noll et al., 1996); (4) subaerial volcanic outgassing and deposition in surface sediments. The influence of each of these processes on transferring As, Tl, Pb, and Bi to the continental crust is considered below.

Juvenile crust formed by partial melting is added to the continental crust by accretion of arcs or oceanic crust or by magmatic intrusion and/or underplating. Element transfer by magmatic processes follows the order of incompatibility. Since the large anomalies of As, Tl, Pb, and Bi do not follow the order of elemental incompatibility, this implies that one of the three nonmelting processes must be responsible for the high As, Tl, Pb, and Bi observed in the continental crust (Figure 9). First, the role of magmatic outgassing lacks the correct chemical signatures to transfer these four elements to the crust. A study of the enrichment factors for each of these elements in Kilauea aerosols found the following order of enrichment: Cd ~ Bi $>$ Tl ~ Sn $>$ As ~ Pb ~ Sb ~ Zn (Mather et al., 2012). Yet the continental crust is not enriched in Cd, Zn, or Sn above their lithophile equivalents (Dy, Fe, and Sm). Enrichments for Re in the continental crust, or depletions in MORB sources, are also not observed while Re is known to be degassed in subaerial lavas (Lassiter, 2003; Norman et al., 2004). Thus, another process must contribute enrichments for As, Tl, Pb, and Bi in the continental crust.

Noll et al. (1996) documented the increase in abundances of As and Pb in arc lavas due to fluid mobility, while abundances of Cu, Zn, Mo, Sn, and W did not increase above lithophile equivalents. Prytulak et al. (2013) did not find evidence of fluid mobile behavior of Tl in the Mariana arc, while Jenner et al. (2012) found positive Tl enrichments (relative to Ce and Pr) from some Lau back-arc lavas and Nielsen et al. (2015) found Tl strongly partitions into the fluid phase at Mariana forearc. Recent Tl isotopic work indicates that the Tl budget of arc lavas are dominated by Tl from pelagic clays from a sediment mélange (Nielsen et al., 2016, 2017; Shu et al., 2017). Jenner et al. (2012) also found correlated enrichments of As, Tl, Pb, and Bi in backarc lavas from the Manus Basin, which were interpreted by Jenner (2017) as evidence of fluid enrichment of As, Tl, Pb, Sb, and Bi to arc crust. Tooth et al. (2013) observed that Bi required higher temperatures than Sb for hydrothermal transport by aqueous fluids in the absence of chlorine. Etschmann et al. (2016) determined that Bi (III) chloride is the predominant mobile species of Bi above 200 °C in hydrothermal processes, so that fluid mobility of Bi is possible in subduction zones.

The same tendency to partition into hydrothermal fluids that gives rise to enrichment of As, Pb, and Bi in arcs, also concentrates these elements in hydrothermal sulfide ores or sediments at mid-oceanic ridges. Obduction of such sediments enriched in hydrothermal ores was proposed to explain the Pb enrichment of the continental crust (Peucker-Ehrenbrink et al., 1994). Bismuth is known to concentrate in Pb ores (Carlin, 2010), so a mechanism that works for Pb enrichment would also work for Bi enrichment in the continental crust. Because Bi data are comparatively scarce, the Pb/Ce ratio (Newsom et al., 1986) provides a powerful constraint with which to evaluate the extraction of As and Bi from the mantle. Both OIBs and MORBs have low Pb/Ce ratios, while continental crust is enriched in Pb/Ce, indicating that the extraction of As, Tl, Pb, and Bi from the MORB source(s) started prior to 2.5 Ga, during a period of Earth history when the operation of modern plate tectonic processes like subduction are controversial (Korenaga, 2013; Tang et al., 2016).

The Sb abundance in the continental crust (Rudnick & Gao, 2003) shows a positive anomaly (×3) relative to Pr-Sm that lacks the complementary depletion in MORBs (Figure 9). The lack of depletion of Sb observed in MORBs in this study stands in contrast to the observed enrichment of Sb in the continental crust (Rudnick & Gao, 2003). This is not well understood at present. Similarly, Figure 9 also shows that the Ag abundance in the continental crust (Rudnick & Gao, 2003) is about ×7 higher than PM, without a complementary Ag depletion in MORBs. Jenner (2017) emphasized the role of sulfide accumulation in the deep crust,

followed by crustal delamination to remove compatible chalcophile and siderophile elements from the continental crust. These processes help understand the lower abundance of Cu, and the higher Ag/Cu ratio in the continental crust, but do not impact the abundances of As, Pb, Tl, and Bi that are not enriched in cumulate sulfide ores.

5. Conclusions

(1) The ratios of Th/U, Nb/U, Ba/Th, and Ba/La in N- and E-MORBs are comparable to the PM values, which cannot be reconciled by a significant addition of AOC that has undergone the loss of fluid-mobile elements (e.g., U, Ba) to the DMM.

(2) A compilation of available data for all chalcophile and siderophile element data allowed refining the ratios of these elements to lithophile elements for each type of MORB. Many low-level chalcophile/lithophile element ratios, including As/Ce, Tl/Ce, Pb/Ce, In/Y, Sn/Sm, W/Ba, and Mo/La, were precisely determined ($< \pm 8\%$, 1σ). The Sb abundances of Jenner and O'Neill (2012) are systematically too low by a factor of 4 relative to our data and that of Kelley et al. (2013) and Jochum and Hofmann (1997). The W/Ba ratio in the present study remains constant even at the lowest values of Ba observed in D-MORBs, comparable in precision to the isotope dilution data from König et al. (2011).

(3) Our new measurements revealed that Sb is most similar to Sm, Mo is most similar to La, and W is most similar to Ba in their compatibilities. The constant ratios of Sb/Sm, Mo/La, and W/Ba of MORBs obtained in this study show no need to invoke core-mantle interaction in MORBs.

(4) The negative anomalies of W, Cd, and Sn in the PM-normalized MORB are caused by the overestimation of these elements in the PM compositions from McDonough and Sun (1995). These anomalies disappear if the updated PM compositions of W (12 ppb, König et al., 2011), Cd (18 ppb, Yi et al., 2000), and Sn (91 ppb, Witt-Eickschen et al., 2009) are used.

(5) Comparison of the MORB compositions with that of the continental crust shows that abundances of As, Tl, Pb, and Bi (but not Sb or Ag) are more depleted in MORB than implied by their lithophile equivalents with the complementary enrichment observed in the continental crust. The chemical signature of this enrichment is shown to be due to neither volcanic outgassing nor magmatic transfer. Fluid mobility in arcs or obduction of seafloor hydrothermal ores is found to be the principal transfer mechanism. The similarity of depletions of As, Tl, Pb, and Bi between each of the MORB types implies that all MORB sources must contain roughly equal amounts of recycled oceanic crust that replenished the nonmobile elements and that this process must have taken place early in Earth history despite controversy over the initiation of modern-style plate tectonics.

Acknowledgments
We thank the Smithsonian Institution (SI) for providing MORB glasses. We thank Cathleen Brown (SI) for help with background information on the AVGDF glasses. We thank Tim Rose (SI) for supplying VG 2 and for discussions on the AVGDF. We thank Katie Kelley for discussions. We thank Gary White for maintaining the laser ablation system in working order. The National High Magnetic Field Laboratory is supported by National Science Foundation through NSF/DMR-1157490 and the State of Florida. We thank Maryjo Brounce, Frances Jenner, and an anonymous reviewer for comments that greatly improved the presentation of the manuscript. We thank Janne Blichert-Toft for her editorial handling. The data set of 319 MORBs analyzed in this study is available from EarthChem library (http://www.earthchem.org/library DOI: 10.1594/IEDA/111192).

References

Anders, E., & Grevesse, N. (1989). Abundances of the elements: Meteoritic and solar. *Geochimica et Cosmochimica Acta*, *53*(1), 197–214. https://doi.org/10.1016/0016-7037(89)90286-X

Andersen, M. B., Elliott, T., Freymuth, H., Sims, K. W. W., Niu, Y., & Kelley, K. A. (2015). The terrestrial uranium isotope cycle. *Nature*, *517*(7534), 356–359. https://doi.org/10.1038/nature14062

Arevalo, R., & McDonough, W. F. (2008). Tungsten geochemistry and implications for understanding the Earth's interior. *Earth and Planetary Science Letters*, *272*(3–4), 656–665. https://doi.org/10.1016/j.epsl.2008.05.031

Arevalo, R., & McDonough, W. F. (2010). Chemical variations and regional diversity observed in MORB. *Chemical Geology*, *271*(1–2), 70–85. https://doi.org/10.1016/j.chemgeo.2009.12.013

Baedecker, P. A., Schaudy, R., Elzie, J. L., Kimberlin, J., & Wasson, J. T. (1971). Trace element studies of rocks and soils from Oceanus Procellarum and Mare Tranquillitatis. *Proceedings of the Lunar Science Conference*, *2*, 1037–1060.

Ballhaus, C., Laurenz, V., Münker, C., Fonseca, R. O. C., Albarède, F., Rohrbach, A., Lagos, M., et al. (2013). The U/Pb ratio of the Earth's mantle—A signature of late volatile addition. *Earth and Planetary Science Letters*, *362*, 237–245. https://doi.org/10.1016/j.epsl.2012.11.049

Bédard, J. H. (2001). Parental magmas of the Nain plutonic suite anorthosites and mafic cumulates: A trace element modelling approach. *Contributions to Mineralogy and Petrology*, *141*(6), 747–771. https://doi.org/10.1007/s004100100268

Brandon, A. D. (1998). Coupled 186Os and 187Os evidence for core-mantle interaction. *Science*, *280*(5369), 1570–1573. https://doi.org/10.1126/science.280.5369.1570

Carlin, J. F., Jr (2010). Bismuth. *USGS 2010* Minerals Yearbook *2010*, 5 pp.

Clague, D. A., Holcomb, R. T., Sinton, J. M., Detrick, R. S., & Torresan, M. E. (1990). Pliocene and Pleistocene alkalic flood basalts on the seafloor north of the Hawaiian Islands. *Earth and Planetary Science Letters*, *98*(2), 175–191. https://doi.org/10.1016/0012-821X(90)90058-6

Coogan, L. A., & O'Hara, M. J. (2015). MORB differentiation: In situ crystallization in replenished-tapped magma chambers. *Geochimica et Cosmochimica Acta*, *158*, 147–161. https://doi.org/10.1016/j.gca.2015.03.010

Courtillot, V., Davaille, A., Besse, J., & Stock, J. (2003). Three distinct types of hotspots in the Earth's mantle. *Earth and Planetary Science Letters*, *205*(3–4), 295–308. https://doi.org/10.1016/S0012-821X(02)01048-8

De Bievre, P., & Taylor, P. D. P. (1993). Table of the isotopic compositions of the elements. *International Journal of Mass Spectrometry and Ion Processes*, *123*(2), 149–166. https://doi.org/10.1016/0168-1176(93)87009-H

Dixon, J. E., Clague, D. A., & Stolper, E. M. (1991). Degassing history of water, sulfur, and carbon in submarine lavas from Kilauea volcano, Hawaii. *The Journal of Geology*, *99*(3), 371–394. https://doi.org/10.1086/629501

Donnelly, K. E., Goldstein, S. L., Langmuir, C. H., & Spiegelman, M. (2004). Origin of enriched ocean ridge basalts and implications for mantle dynamics. *Earth and Planetary Science Letters*, *226*(3–4), 347–366. https://doi.org/10.1016/j.epsl.2004.07.019

Eiler, J. M., Schiano, P., Kitchen, N., & Stolper, E. M. (2000). Oxygen-isotope evidence for recycled crust in the sources of mid-ocean-ridge basalts. *Nature*, *403*(6769), 530–534. https://doi.org/10.1038/35000553

Eisele, J., Sharma, M., Galer, S. J., Blichert-Toft, J., Devey, C. W., & Hofmann, A. W. (2002). The role of sediment recycling in EM-1 inferred from Os, Pb, Hf, Nd, Sr isotope and trace element systematics of the Pitcairn hotspot. *Earth and Planetary Science Letters*, *196*(3-4), 197–212. https://doi.org/10.1016/S0012-821X(01)00601-X

Escrig, S., Schiano, P., Schilling, J.-G., & Allègre, C. (2005). Rhenium–osmium isotope systematics in MORB from the southern Mid-Atlantic Ridge (40°–50°S). *Earth and Planetary Science Letters*, *235*(3–4), 528–548. https://doi.org/10.1016/j.epsl.2005.04.035

Etschmann, B. E., Liu, W., Pring, A., Grundler, P. V., Tooth, B., Borg, S., Testemale, D., et al. (2016). The role of Te (IV) and Bi (III) chloride complexes in hydrothermal mass transfer: An X-ray absorption spectroscopic study. *Chemical Geology*, *425*, 37–51. https://doi.org/10.1016/j.chemgeo.2016.01.015

Gaboardi, M., & Humayun, M. (2009). Elemental fractionation during LA-ICP-MS analysis of silicate glasses: Implications for matrix-independent standardization. *Journal of Analytical Atomic Spectrometry*, *24*(9), 1188. https://doi.org/10.1039/b900876d

Gale, A., Dalton, C. A., Langmuir, C. H., Su, Y., & Schilling, J.-G. (2013). The mean composition of ocean ridge basalts. *Geochemistry, Geophysics, Geosystems*, *14*, 489–518. https://doi.org/10.1029/2012GC004334

Gale, A., Langmuir, C. H., & Dalton, C. A. (2014). The global systematics of ocean ridge basalts and their origin. *Journal of Petrology*, *55*(6), 1051–1082. https://doi.org/10.1093/petrology/egu017

Galer, S. J., & O'Nions, R. K. (1986). Magmagenesis and the mapping of chemical and isotopic variations in the mantle. *Chemical Geology*, *56*(1-2), 45–61. https://doi.org/10.1016/0009-2541(86)90109-9

Gao, S., Luo, T.-C., Zhang, B.-R., Zhang, H.-F., Han, Y., Zhao, Z.-D., & Hu, Y.-K. (1998). Chemical composition of the continental crust as revealed by studies in East China. *Geochimica et Cosmochimica Acta*, *62*(11), 1959–1975. https://doi.org/10.1016/S0016-7037(98)00121-5

Grove, T. L., & Bryan, W. B. (1983). Fractionation of pyroxene-phyric MORB at low pressure: An experimental study. *Contributions to Mineralogy and Petrology*, *84*(4), 293–309. https://doi.org/10.1007/BF01160283

Hauri, E. H., & Hart, S. R. (1997). Rhenium abundances and systematics in oceanic basalts. *Chemical Geology*, *139*(1–4), 185–205. https://doi.org/10.1016/S0009-2541(97)00035-1

Heinrichs, H., Schulz-Dobrick, B., & Wedepohl, K. H. (1980). Terrestrial geochemistry of Cd, Bi, Tl, Pb, Zn and Rb. *Geochimica et Cosmochimica Acta*, *44*(10), 1519–1533. https://doi.org/10.1016/0016-7037(80)90116-7

Helz, R. T., Clague, D. A., Mastin, L. G., & Rose, T. R. (2014). Electron microprobe analyses of glasses from Kilauea Tephra units, Kilauea Volcano, Hawaii (Open-File Report). U.S. Geological Survey.

Hémond, C., Hofmann, A. W., Vlastélic, I., & Nauret, F. (2006). Origin of MORB enrichment and relative trace element compatibilities along the Mid-Atlantic Ridge between 10° and 24°N. *Geochemistry, Geophysics, Geosystems*, *7*, Q12010. https://doi.org/10.1029/2006GC001317

Hertogen, J., Janssens, M.-J., & Palme, H. (1980). Trace elements in ocean ridge basalt glasses: Implications for fractionations during mantle evolution and petrogenesis. *Geochimica et Cosmochimica Acta*, *44*(12), 2125–2143. https://doi.org/10.1016/0016-7037(80)90209-4

Hirschmann, M. M., & Stolper, E. M. (1996). A possible role for garnet pyroxenite in the origin of the "garnet signature" in MORB. *Contributions to Mineralogy and Petrology*, *124*(2), 185–208. https://doi.org/10.1007/s004100050184

Hofmann, A. W. (1988). Chemical differentiation of the Earth: The relationship between mantle, continental crust, and oceanic crust. *Earth and Planetary Science Letters*, *90*(3), 297–314. https://doi.org/10.1016/0012-821X(88)90132-X

Hu, Z., & Gao, S. (2008). Upper crustal abundances of trace elements: A revision and update. *Chemical Geology*, *253*(3–4), 205–221. https://doi.org/10.1016/j.chemgeo.2008.05.010

Humayun, M. (2012). Chondrule cooling rates inferred from diffusive profiles in metal lumps from the Acfer 097 CR2 chondrite: Diffusive profiles in CR chondrite metal lumps. *Meteoritics & Planetary Science*, *47*(7), 1191–1208. https://doi.org/10.1111/j.1945-5100.2012.01371.x

Humayun, M., Davis, F. A., & Hirschmann, M. M. (2010). Major element analysis of natural silicates by laser ablation ICP-MS. *Journal of Analytical Atomic Spectrometry*, *25*(7), 998. https://doi.org/10.1039/c001391a

Humayun, M., Simon, S. B., & Grossman, L. (2007). Tungsten and hafnium distribution in calcium–aluminum inclusions (CAIs) from Allende and Efremovka. *Geochimica et Cosmochimica Acta*, *71*(18), 4609–4627. https://doi.org/10.1016/j.gca.2007.07.014

Jarosewich, E. (1975). Chemical composition of two microprobe standards. *Smithsonian Contrib. Earth Science*, *14*, 85–86.

Jenner, F. E. (2017). Cumulate causes for the low contents of sulfide-loving elements in the continental crust. *Nature Geoscience*, *10*(7), 524–529. https://doi.org/10.1038/ngeo2965

Jenner, F. E., Arculus, R. J., Mavrogenes, J. A., Dyriw, N. J., Nebel, O., & Hauri, E. H. (2012). Chalcophile element systematics in volcanic glasses from the northwestern Lau Basin. *Geochemistry, Geophysics, Geosystems*, *13*, Q06014. https://doi.org/10.1029/2012GC004088

Jenner, F. E., & O'Neill, H. S. C. (2012). Analysis of 60 elements in 616 ocean floor basaltic glasses. *Geochemistry, Geophysics, Geosystems*, *13*, Q02005. https://doi.org/10.1029/2011GC004009

Jochum, K. P., & Hofmann, A. W. (1997). Constraints on Earth evolution from antimony in mantle-derived rocks. *Chemical Geology*, *139*(1-4), 39–49. https://doi.org/10.1016/S0009-2541(97)00032-6

Jochum, K. P., Hofmann, A. W., & Seufert, H. M. (1993). Tin in mantle-derived rocks: Constraints on Earth evolution. *Geochimica et Cosmochimica Acta*, *57*(15), 3585–3595. https://doi.org/10.1016/0016-7037(93)90141-I

Jochum, K. P., & Nohl, U. (2008). Reference materials in geochemistry and environmental research and the GeoReM database. *Chemical Geology*, *253*(1–2), 50–53. https://doi.org/10.1016/j.chemgeo.2008.04.002

Jochum, K. P., Stoll, B., Herwig, K., Willbold, M., Hofmann, A. W., Amini, M., Aarburg, S., et al. (2006). MPI-DING reference glasses for in situ microanalysis: New reference values for element concentrations and isotope ratios. *Geochemistry, Geophysics, Geosystems*, *7*, Q02008. https://doi.org/10.1029/2005GC001060

Jochum, K. P., Weis, U., Stoll, B., Kuzmin, D., Yang, Q., Raczek, I., Jacob, D. E., et al. (2011). Determination of reference values for NIST SRM 610–617 glasses Following ISO Guidelines. *Geostandards and Geoanalytical Research*, *35*(4), 397–429. https://doi.org/10.1111/j.1751-908X.2011.00120.x

Jochum, K. P., Willbold, M., Raczek, I., Stoll, B., & Herwig, K. (2005). Chemical characterisation of the USGS reference glasses GSA-1G, GSC-1G, GSD-1G, GSE-1G, BCR-2G, BHVO-2G and BIR-1G using EPMA, ID-TIMS, ID-ICP-MS and LA-ICP-MS. *Geostandards and Geoanalytical Research*, *29*(3), 285–302. https://doi.org/10.1111/j.1751-908X.2005.tb00901.x

Kelley, K. A., Kingsley, R., & Schilling, J.-G. (2013). Composition of plume-influenced mid-ocean ridge lavas and glasses from the mid-Atlantic ridge, East Pacific rise, Galápagos Spreading Center, and Gulf of Aden. *Geochemistry, Geophysics, Geosystems*, *14*, 223–242. https://doi.org/10.1002/ggge.20049

Kelley, K. A., Plank, T., Ludden, J., & Staudigel, H. (2003). Composition of altered oceanic crust at ODP sites 801 and 1149. *Geochemistry, Geophysics, Geosystems*, *4*(6), 8910. https://doi.org/10.1029/2002GC000435

Kessel, R., Schmidt, M. W., Ulmer, P., & Pettke, T. (2005). Trace element signature of subduction-zone fluids, melts and supercritical liquids at 120–180 km depth. *Nature*, *437*(7059), 724–727. https://doi.org/10.1038/nature03971

Kiseeva, E. S., & Wood, B. J. (2013). A simple model for chalcophile element partitioning between sulphide and silicate liquids with geochemical applications. *Earth and Planetary Science Letters*, *383*, 68–81. https://doi.org/10.1016/j.epsl.2013.09.034

Klein, E. M., & Langmuir, C. H. (1987). Global correlations of ocean ridge basalt chemistry with axial depth and crustal thickness. *Journal of Geophysical Research*, *92*(B8), 8089. https://doi.org/10.1029/JB092iB08p08089

König, S., Münker, C., Hohl, S., Paulick, H., Barth, A. R., Lagos, M., Pfänder, J., et al. (2011). The Earth's tungsten budget during mantle melting and crust formation. *Geochimica et Cosmochimica Acta*, *75*(8), 2119–2136. https://doi.org/10.1016/j.gca.2011.01.031

Korenaga, J. (2013). Initiation and evolution of plate tectonics on Earth: Theories and observations. *Annual Review of Earth and Planetary Sciences*, *41*(1), 117–151. https://doi.org/10.1146/annurev-earth-050212-124208

Langmuir, C. H., Klein, E. M., & Plank, T. (1993). Petrological systematics of mid-ocean ridge basalts: Constraints on melt generation beneath ocean ridges. *Mantle Flow and Melt Generation at Mid-Ocean Ridges*, 183–280.

Lassiter, J. (2003). Rhenium volatility in subaerial lavas: Constraints from subaerial and submarine portions of the HSDP-2 Mauna kea drillcore. *Earth and Planetary Science Letters*, *214*(1–2), 311–325. https://doi.org/10.1016/S0012-821X(03)00385-6

Lissenberg, C. J., & MacLeod, C. J. (2016). A reactive porous flow control on mid-ocean ridge magmatic evolution. *Journal of Petrology*, *57*(11–12), 2195–2220. https://doi.org/10.1093/petrology/egw074

Lyubetskaya, T., & Korenaga, J. (2007). Chemical composition of Earth's primitive mantle and its variance: 1. Method and results. *Journal of Geophysical Research*, *112*, B03211. https://doi.org/10.1029/2005JB004223

Mann, U., Frost, D. J., & Rubie, D. C. (2009). Evidence for high-pressure core-mantle differentiation from the metal–silicate partitioning of lithophile and weakly-siderophile elements. *Geochimica et Cosmochimica Acta*, *73*(24), 7360–7386. https://doi.org/10.1016/j.gca.2009.08.006

Mather, T. A., Witt, M. L. I., Pyle, D. M., Quayle, B. M., Aiuppa, A., Bagnato, E., Martin, R. S., et al. (2012). Halogens and trace metal emissions from the ongoing 2008 summit eruption of Kīlauea volcano, Hawai'i. *Geochimica et Cosmochimica Acta*, *83*, 292–323. https://doi.org/10.1016/j.gca.2011.11.029

McDonough, W. F., & Sun, S. S. (1995). The composition of the earth. *Chemical Geology*, *120*(3–4), 223–253. https://doi.org/10.1016/0009-2541(94)00140-4

Melson, W. G., Vallier, T. L., Wright, T. L., Byerly, G., & Nelen, J. (1976). Chemical diversity of abyssal volcanic glass erupted along Pacific, Atlantic, and Indian Ocean sea-floor spreading centers. In G. H. Sutton, M. H. Manghnani, R. Moberly, & E. U. Mcafee (Eds.), *Geophysical Monograph Series* (pp. 351–367). Washington, DC: American Geophysical Union. https://doi.org/10.1029/GM019p0351

Melson, W. G., O'Hearn, T., & Jarosewich, E. (2002). A data brief on the Smithsonian abyssal volcanic glass data file. *Geochemistry, Geophysics, Geosystems*, *3*(4), 1023. https://doi.org/10.1029/2001GC000249

Münker, C., Pfänder, J. A., Weyer, S., Büchl, A., Kleine, T., & Mezger, K. (2003). Evolution of planetary cores and the Earth-Moon system from Nb/ta systematics. *Science*, *301*(5629), 84–87. https://doi.org/10.1126/science.108466

Newsom, H. E., White, W. M., Jochum, K. P., & Hofmann, A. W. (1986). Siderophile and chalcophile element abundances in oceanic basalts, Pb isotope evolution and growth of the Earth's core. *Earth and Planetary Science Letters*, *80*(3–4), 299–313. https://doi.org/10.1016/0012-821X(86)90112-3

Newsom, H. E., Sims, K. W., Noll, P. D. Jr., Jaeger, W. L., Maehr, S. A., & Beserra, T. B. (1996). The depletion of tungsten in the bulk silicate earth: Constraints on core formation. *Geochimica et Cosmochimica Acta*, *60*(7), 1155–1169. https://doi.org/10.1016/0016-7037(96)00029-4

Nielsen, S. G., Klein, F., Kading, T., Blusztajn, J., & Wickham, K. (2015). Thallium as a tracer of fluid–rock interaction in the shallow Mariana forearc. *Earth and Planetary Science Letters*, *430*, 416–426. https://doi.org/10.1016/j.epsl.2015.09.001

Nielsen, S. G., & Lee, C.-T. A. (2013). Determination of thallium in the USGS glass reference materials BIR-1G, BHVO-2G and BCR-2G and application to quantitative Tl concentrations by LA-ICP-MS. *Geostandards and Geoanalytical Research*, *37*(3), 337–343. https://doi.org/10.1111/j.1751-908x.2012.00203.x

Nielsen, S. G., Prytulak, J., Blusztajn, J., Shu, Y., Auro, M., Regelous, M., & Walker, J. (2017). Thallium isotopes as tracers of recycled materials in subduction zones: Review and new data for lavas from Tonga-Kermadec and Central America. *Journal of Volcanology and Geothermal Research*, *339*, 23–40. https://doi.org/10.1016/j.jvolgeores.2017.04.024

Nielsen, S. G., Shimizu, N., Lee, C.-T. A., & Behn, M. D. (2014). Chalcophile behavior of thallium during MORB melting and implications for the sulfur content of the mantle. *Geochemistry, Geophysics, Geosystems*, *15*, 4905–4919. https://doi.org/10.1002/2014GC005536

Nielsen, S. G., Yogodzinski, G., Prytulak, J., Plank, T., Kay, S. M., Kay, R. W., Blusztajn, J., et al. (2016). Tracking along-arc sediment inputs to the Aleutian arc using thallium isotopes. *Geochimica et Cosmochimica Acta*, *181*, 217–237. https://doi.org/10.1016/j.gca.2016.03.010

Niu, Y., & O'Hara, M. J. (2008). Global correlations of ocean ridge basalt chemistry with axial depth: A new perspective. *Journal of Petrology*, *49*(4), 633–664. https://doi.org/10.1093/petrology/egm051

Niu, Y., & O'Hara, M. J. (2009). MORB mantle hosts the missing Eu (Sr, Nb, ta and Ti) in the continental crust: New perspectives on crustal growth, crust–mantle differentiation and chemical structure of oceanic upper mantle. *Lithos*, *112*(1–2), 1–17. https://doi.org/10.1016/j.lithos.2008.12.009

Niu, Y., Regelous, M., Wendt, I. J., Batiza, R., & O'Hara, M. J. (2002). Geochemistry of near-EPR seamounts: importance of source vs. process and the origin of enriched mantle component. *Earth and Planetary Science Letters*, *1999*(3–4), 327–345. https://doi.org/10.1016/S0012-821X(02)00591-5

Noll, P. D. Jr., Newsom, H. E., Leeman, W. P., & Ryan, J. G. (1996). The role of hydrothermal fluids in the production of subduction zone magmas: Evidence from siderophile and chalcophile trace elements and boron. *Geochimica et Cosmochimica Acta*, *60*(4), 587–611. https://doi.org/10.1016/0016-7037(95)00405-X

Norman, M. D., & Garcia, M. O. (1999). Primitive magmas and source characteristics of the Hawaiian plume: petrology and geochemistry of shield picrites. *Earth and Planetary Science Letters*, *168*(1), 27–44.

Norman, M. D., Garcia, M. O., & Bennett, V. C. (2004). Rhenium and chalcophile elements in basaltic glasses from Ko'olau and Moloka'i volcanoes: Magmatic outgassing and composition of the Hawaiian plume. *Geochimica et Cosmochimica Acta*, *68*(18), 3761–3777. https://doi.org/10.1016/j.gca.2004.02.025

O'Neill, H. S. C., & Jenner, F. E. (2012). The global pattern of trace-element distributions in ocean floor basalts. *Nature*, *491*(7426), 698–704. https://doi.org/10.1038/nature11678

O'Neill, H. S. C., & Jenner, F. E. (2016). Causes of the compositional variability among ocean floor basalts. *Journal of Petrology*, *57*(11–12), 2163–2194. https://doi.org/10.1093/petrology/egx001

Palme, H., & O'Neill, H. S. C. (2003). Cosmochemical estimates of mantle composition. *The Mantle and Core: Treatise on Geochemistry*, *2*, 1–38.

Perfit, M. R. (2001). Mid-ocean ridge geochemistry and petrology. In J. Steele, S. Thorp, & K. Turekian (Eds.), *Encyclopedia of Ocean Sciences* (pp. 1778–1788). San Diego, CA: Academic Press. https://doi.org/10.1006/rwos.2001.0096

Peucker-Ehrenbrink, B., Hofmann, A. W., & Hart, S. R. (1994). Hydrothermal lead transfer from mantle to continental crust: The role of metalliferous sediments. *Earth and Planetary Science Letters*, *125*(1–4), 129–142. https://doi.org/10.1016/0012-821X(94)90211-9

Prytulak, J., Nielsen, S. G., Plank, T., Barker, M., & Elliott, T. (2013). Assessing the utility of thallium and thallium isotopes for tracing subduction zone inputs to the Mariana arc. *Chemical Geology*, *345*, 139–149. https://doi.org/10.1016/j.chemgeo.2013.03.003

Qin, L., & Humayun, M. (2008). The Fe/Mn ratio in MORB and OIB determined by ICP-MS. *Geochimica et Cosmochimica Acta*, *72*(6), 1660–1677. https://doi.org/10.1016/j.gca.2008.01.012

Reisberg, L., Zindler, A., Marcantonio, F., White, W., Wyman, D., & Weaver, B. (1993). Os isotope systematics in ocean island basalts. *Earth and Planetary Science Letters*, *120*(3–4), 149–167. https://doi.org/10.1016/0012-821X(93)90236-3

Righter, K., Danielson, L. R., Pando, K. M., Williams, J., Humayun, M., Hervig, R. L., & Sharp, T. G. (2015). Highly siderophile element (HSE) abundances in the mantle of Mars are due to core formation at high pressure and temperature. *Meteoritics & Planetary Science*, *50*(4), 604–631. https://doi.org/10.1111/maps.12393

Righter, K., Pando, K. M., Danielson, L., & Lee, C.-T. (2010). Partitioning of Mo, P and other siderophile elements (cu, Ga, Sn, Ni, co, Cr, Mn, V, and W) between metal and silicate melt as a function of temperature and silicate melt composition. *Earth and Planetary Science Letters*, *291*(1–4), 1–9. https://doi.org/10.1016/j.epsl.2009.12.018

Rubie, D. C., Gessmann, C. K., & Frost, D. J. (2004). Partitioning of oxygen during core formation on the earth and Mars. *Nature*, *429*(6987), 58–61. https://doi.org/10.1038/nature02473

Rudnick, R. L., & Gao, S. (2003). Composition of the continental crust. *Treatise on Geochemistry*, *3*, 659.

Salters, V. J. M., & Stracke, A. (2004). Composition of the depleted mantle. *Geochemistry, Geophysics, Geosystems*, *5*, Q05B07. https://doi.org/10.1029/2003GC000597

Schiano, P., Birck, J.-L., & Allègre, C. J. (1997). Osmium-strontium-neodymium-lead isotopic covariations in mid-ocean ridge basalt glasses and the heterogeneity of the upper mantle. *Earth and Planetary Science Letters*, *150*(3-4), 363–379. https://doi.org/10.1016/S0012-821X(97)00098-8

Schilling, J. G. (1973). Iceland mantle plume: Geochemical study of Reykjanes ridge. *Nature*, *242*, 565–571. https://doi.org/10.1038/242565a

Schilling, J. G. (1985). Upper mantle heterogeneities and dynamics. *Nature*, *314*, 62–67. https://doi.org/10.1038/314062a0

Schilling, J. G., & Kingsley, R. H. (2017). Platinum–group elements (PGE), Re, Ni, Cu, Ag and Cd Variations along the Reykjanes Ridge and Iceland South–West Neovolcanic Rift Zone, from 50 N to 65 N: Implications on sulfide bearing PGE mantle source heterogeneities and partial melting effects [data set]. *Interdisciplinary Earth Data Alliance (IEDA)*. https://doi.org/10.1594/IEDA/100712

Shorttle, O., Rudge, J. F., Maclennan, J., & Rubin, K. H. (2016). A statistical description of concurrent mixing and crystallization during MORB differentiation: Implications for trace element enrichment. *Journal of Petrology*, *57*(11–12), 2127–2162. https://doi.org/10.1093/petrology/egw056

Shu, Y., Nielsen, S. G., Zeng, Z., Shinjo, R., Blusztajn, J., Wang, X., & Chen, S. (2017). Tracing subducted sediment inputs to the Ryukyu arc-Okinawa Trough system: Evidence from thallium isotopes. *Geochimica et Cosmochimica Acta*, *217*, 462–491. https://doi.org/10.1016/j.gca.2017.08.035

Sims, K. W. W., Newsom, H. E., & Gladney, E. S. (1990). Chemical fractionation during formation of the Earth's core and continental crust: Clues from As, Sb, W, and Mo. In H. E. Newsom & J. H. Jones (Eds.), *Origin of Earth* (pp. 291–317). New York: Oxford University Press.

Sobolev, A. V., Hofmann, A. W., Kuzmin, D. V., Yaxley, G. M., Arndt, N. T., Chung, S.-L., Danyushevsky, L. V., et al. (2007). The amount of recycled crust in sources of mantle-derived melts. *Science*, *316*(5823), 412–417. https://doi.org/10.1126/science. 1138113

Stolper, E., Sherman, S., Garcia, M., Baker, M., & Seaman, C. (2004). Glass in the submarine section of the HSDP2 DRILL CORE, Hilo, HAWAII: HSDP2 DRILL CORE, HAWAII. *Geochemistry, Geophysics, Geosystems*, *5*, Q07G15. https://doi.org/10.1029/2003GC000553

Stracke, A. (2012). Earth's heterogeneous mantle: A product of convection-driven interaction between crust and mantle. *Chemical Geology*, *330–331*, 274–299. https://doi.org/10.1016/j.chemgeo.2012.08.007

Stracke, A., Bizimis, M., & Salters, V. J. M. (2003). Recycling oceanic crust: Quantitative constraints. *Geochemistry, Geophysics, Geosystems*, *4*(3), 8003. https://doi.org/10.1029/2001GC000223

Stracke, A., & Bourdon, B. (2009). The importance of melt extraction for tracing mantle heterogeneity. *Geochimica et Cosmochimica Acta*, *73*(1), 218–238. https://doi.org/10.1016/j.gca.2008.10.015

Sun, S. S., & McDonough, W. F. (1989). Chemical and isotopic systematics of oceanic basalts: Implications for mantle composition and processes. *Geological Society, London, Special Publications*, *42*(1), 313–345. https://doi.org/10.1144/GSL.SP.1989.042.01.19

Sun, W., Bennett, V. C., Eggins, S. M., Arculus, R. J., & Perfit, M. R. (2003). Rhenium systematics in submarine MORB and back-arc basin glasses: laser ablation ICP-MS results. *Chemical Geology*, *196*(1–4), 259–281. https://doi.org/10.1016/S0009-2541(02)00416-3

Tang, M., Chen, K., & Rudnick, R. L. (2016). Archean upper crust transition from mafic to felsic marks the onset of plate tectonics. *Science*, *351*(6271), 372–375. https://doi.org/10.1126/science.aad5513

Taylor, S. R., & McLennan, S. M. (1995). The geochemical evolution of the continental crust. *Reviews of Geophysics*, *33*(2), 241–265. https://doi.org/10.1029/95RG00262

Tooth, B., Etschmann, B., Pokrovski, G. S., Testemale, D., Hazemann, J.-L., Grundler, P. V., & Brugger, J. (2013). Bismuth speciation in hydrothermal fluids: An X-ray absorption spectroscopy and solubility study. *Geochimica et Cosmochimica Acta*, *101*, 156–172. https://doi.org/10.1016/j.gca.2012.10.020

Ulrich, M., Hémond, C., Nonnotte, P., & Jochum, K. P. (2012). OIB/seamount recycling as a possible process for E-MORB genesis. *Geochemistry, Geophysics, Geosystems*, https://doi.org/10.1029/2012GC004078, *13*, Q0AC19.

Van Orman, J. A., Grove, T. L., & Shimizu, N. (2001). Rare earth element diffusion in diopside: Influence of temperature, pressure, and ionic radius, and an elastic model for diffusion in silicates. *Contributions to Mineralogy and Petrology*, *141*(6), 687–703. https://doi.org/10.1007/s004100100269

Wade, J., Wood, B. J., & Tuff, J. (2012). Metal–silicate partitioning of Mo and W at high pressures and temperatures: Evidence for late accretion of sulphur to the Earth. *Geochimica et Cosmochimica Acta*, *85*, 58–74. https://doi.org/10.1016/j.gca.2012.01.010

Wang, Z., & Becker, H. (2015). Abundances of Ag and Cu in mantle peridotites and the implications for the behavior of chalcophile elements in the mantle. *Geochimica et Cosmochimica Acta*, *160*, 209–226. https://doi.org/10.1016/j.gca.2015.04.006

Witt-Eickschen, G., Palme, H., O'Neill, H. S. C., & Allen, C. M. (2009). The geochemistry of the volatile trace elements As, Cd, Ga, In and Sn in the Earth's mantle: New evidence from in situ analyses of mantle xenoliths. *Geochimica et Cosmochimica Acta*, *73*(6), 1755–1778. https://doi.org/10.1016/j.gca.2008.12.013

Wood, B. J., Kiseeva, E. S., & Mirolo, F. J. (2014). Accretion and core formation: The effects of sulfur on metal–silicate partition coefficients. *Geochimica et Cosmochimica Acta*, *145*, 248–267. https://doi.org/10.1016/j.gca.2014.09.002

Workman, R. K., & Hart, S. R. (2005). Major and trace element composition of the depleted MORB mantle (DMM). *Earth and Planetary Science Letters*, *231*(1-2), 53–72. https://doi.org/10.1016/j.epsl.2004.12.005

Yang, S., Humayun, M., Righter, K., Jefferson, G., Fields, D., & Irving, A. J. (2015). Siderophile and chalcophile element abundances in shergottites: Implications for Martian core formation. *Meteoritics & Planetary Science*, *50*(4), 691–714. https://doi.org/10.1111/maps.12384

Yi, W., Halliday, A. N., Alt, J. C., Lee, D.-C., Rehkämper, M., Garcia, M. O., Langmuir, C. H., et al. (2000). Cadmium, indium, tin, tellurium, and sulfur in oceanic basalts: Implications for chalcophile element fractionation in the Earth. *Journal of Geophysical Research*, *105*(B8), 18,927–18,948. https://doi.org/10.1029/2000JB900152

York, D., Evensen, N. M., Martı´nez, M. L., & De Basabe Delgado, J. (2004). Unified equations for the slope, intercept, and standard errors of the best straight line. *American Journal of Physics*, *72*(3), 367–375. 1632486, https://doi.org/10.1119/1.1632486

Zhang, H. L., Cottrell, E., Solheid, P. A., Kelley, K. A., & Hirschmann, M. M. (2018). Determination of Fe 3+/ΣFe of XANES basaltic glass standards by Mössbauer spectroscopy and its application to the oxidation state of iron in MORB. *Chemical Geology*, *479*, 166–175. https://doi.org/10.1016/j.chemgeo.2018.01.006

Zindler, A., Staudigel, H., & Batiza, R. (1984). Isotope and trace element geochemistry of young Pacific seamounts: Implications for the scale of upper mantle heterogeneity. *Earth and Planetary Science Letters*, *70*(2), 175–195. https://doi.org/10.1016/0012-821X(84)90004-9